The Islamic University of Gaza

Higher Education Deanship

Faculty of Engineering

Civil Engineering Department

Infrastructure Engineering

الجامعة الإسلامية – غزة

عمادة الدراسات العليا

كلية الهندسة

قسم الهندسة المدنية

البنى التحتية

تقنيات التصحيح المكاني ثنائي الأبعاد لصور الأقمار الصناعي (مدينة غزة: حالة دراسية)

Two Dimensional Geometric Rectification Techniques for Remote Sensing Satellite Images (Gaza City as a Case Study)

Submitted by:

AbdelMohsen Ahmad Muhaisen

Supervised by:

Dr. Maher El-Hallaq

A Thesis Submitted in Partial Fulfillment of Requirements for the Degree of Master in Infrastructure Engineering

١٤٣٧ هـ ـ ٢٠١٦ م

DEDICATION

This research is dedicated to my Father - may ALLAH grant him mercy- and my Mother for their infinite support and encouragement,

To my Wife, Son and Daughter,

To my Family,

To all whom we respect and esteem wherever.

ACKNOWLEDGEMENT

ملخص الدراسة

تحتوي بيانات الصور الجوية الخام على تشوهات هندسية بنسب متفاوتة مما يؤثر على درجة دقتها الهندسية ، وهذه التشوهات يمكن تصنيفها إما تشوهات منتظمة أو تشوهات غير منتظمة (عشوائية).

ويمكن معالجة تصحيح التشوهات المنتظمة بتطبيق المعادلات والنماذج الرياضية وتصحيحها رياضيا، أما التشوهات الغير منتظمة (العشوائية) فيتم تصحيحها من خلال توقيع وتوزيع عدد من النقاط الأرضية على أرض الواقع وربطها بالصورة الجوية و القيام بعملية التصحيح الهندسي لها.

لذلك ، فإننا من خلال البحث تطرقنا لعملية التصحيح الهندسي للصور الجوية من خلال تطبيق النماذج الرياضية على الصورة الجوية للحصول على أفضل نتيجة ومن خلال هذه النماذج، وكذلك من خلال توقيع نقاط تحكم أرضية على أرض الواقع وربط النقاط بعد ذلك بمكانها على الصورة الجوية، ليتم بعدها عملية التصحيح من خلال البرنامج المستخدم.

وفي هذا البحث فقد حصلنا على صورة جوية لمدينة غزة لاستخدامها كحالة دراسية وكذلك تم أخذ وقياس ٣٨ نقطة تحكم أرضية والتي كانت مقسمة لمجموعتين، المجموعة الأولى عبارة عن ٢٦ نقطة تحكم أرضية لاستخدامها في عملية التصحيح، والمجموعة الأخرى عبارة عن ١٢ نقطة تحكم أرضية للتأكد من دقة عملية التصحيح وكل ذلك تم من خلال برنامج حاسوبي متخصص في عمليات التصحيح الجوية وهو برنامج Erdas Imgaine Program لعملية التصحيح والتحليل.

وبشكل عام فإن النموذج الرياضي متعدد الحدود من الدرجة الثالثة قد أعطى أفضل النتائج من حيث الدقة وذلك من خلال أخذ العديد من النماذج بدرجات مختلفة.

وكذلك كان هناك ارتباط وثيق وواضح بين عدد نقاط التحكم الأرضية المستخدم والدقة الناتجة عن عملية التصحيح وقد تبين أن عدد النقاط الأرضية يتناسب تناسبا طرديا مع دقة عملية التصحيح لحد معين.

ABSTRACT

Every satellite image has some distortions that affect the geometric accuracy of these images, These distortions are classed in two groups; systematic and non-systematic distortions. The systematic distortions are corrected by applying formulas derived by modeling the source of the distortions mathematically.

Non-systematic distortions, and residual unknown systematic distortions are corrected by analysis of well-distributed ground control points (GCPs) which occurring on the satellite image. The satellite images are delivered after applying some correction processes like radiometric- distortions, but some of these images must be rectified to remove the other types of distortions, so rectification processes are applied.

To apply the rectification processes, it is necessary to acquire the fundamental model of the satellite and applying different mathematical models. These models relate between the point on the image and its conjugate on the earth, and using several models to give the best accuracy.

For this research, a satellite image for Gaza City-Palestine was used. These 38 GCPs are collected and read which are divided to 26 control points for the rectification process and 12 control points as check points to assure the accuracy of the process. Erdas Imgaine Program was used as software at the rectification and analysis process.

In general, it is found that the third order polynomial gives the best results. The effect of GCPs number on resulted accuracy was studied. The rectification operation is repeated by reducing the number of the GCPs gradually in the image. It is found that the accuracy of rectification is directly proportional with the number of GCPS.

LIST OF CONTENTS

vi

LIST OF ABBREVIATIONS

AVIRIS	Airborne Visible Infrared Imaging Spectrometer
CAD	Computer Aided Design
CCM	Canada Centre for Mapping
CCRS	Canada Centre for Remote Sensing
CIA	Central Intelligence Agency
CIR	Color-Infrared Photography
DEM	Digital Elevation Model
DLT	Direct Linear Transformation
DN	Digital Number
EMR	Electromagnetic Radiation
EO	Exterior Orientation
ERDAS	Earth Resources Data Analysis System
EROS	Earth Resources Observation Systems
ETM	Enhanced Thematic Mapper
FOV	Field of View
GCPs	Ground Control Points
GIS	Geographic Information System
GPS	Global Positioning System
HRMSI	High Resolution Multispectral Stereo Imager
HRSI	High Resolution Satellite Image
ID	Identification umber
IFOV	Instantaneous Field of View
MSL	Mean sea level
MSS	Multispectral Scanner
NASA	National Aeronautics and Space Administration
NOAA	National Oceanic and Atmospheric Administration
NRO	The National Reconnaissance Office
RMSE	Root Mean Square Error
RPC	Rational Polynomial Coefficients
RS	Remote Sensing
SAR	Synthetic-Aperture Radar
SPOT	System Propitiate d Observation de *la* Terra
TM	Thematic Mapper
USAF	The United States Air Force
USGS	U.S. Geological Survey

LIST OF TABLES

LIST OF FIGURES

xi

1 CHAPTER 1: INTRODUCTION

1.1 Scope

This chapter is intended to give a brief introduction of research problem emphasizing the importance of two dimensional geometric rectification techniques for remote sensing satellite images using the mathematical models with ERDAS software program to have the best accuracy of the images. It gives a description of the research importance, scope, objectives, methodology and deliverables as well as thesis organization.

1.2 Background

Remote Sensing is the science of obtaining information about objects or areas from a distance, typically from aircraft or satellites and one of the best definitions of Remote sensing was " a tool or technique similar to mathematics. Using sensors to measure the amount of electromagnetic radiation (EMR) exiting an object or geographic area from a distance and then extracting valuable information from the data using mathematically and statistically based algorithms is a scientific activity. It functions in harmony with other spatial data-collection techniques or tools of the mapping sciences, including cartography and geographic information systems (GIS)" (Clarke, 2001).

For Remote Sensing applications, new systems of high resolution satellites were lunched to announce for the beginning of new era of high resolution systems, The most famous satellites in this field are IKONOS , LANDSAT , GeoEye , WorldView , FORMOSAT-2 , ALOS , CARTOSAT, SPOT-5 and QuickBird. These systems are used to gather and give a high resolution satellite images with different resolution according to each satellite specifications.

An important process which must be applied on satellite images called geometric rectification processes which can remove the distortions that resulted from many reasons such as systematic and non-systematic distortions.

The rectification processes produce a rectified image, and to perform these processes, software program ERDAS Imagine Program will be used, It's one of the most famous remote sensing application initially released in 1978, ERDAS designed for geospatial

www.manaraa.com

applications and the latest version of the software is in this year 2015 (Wikipedia, 2014).

Also, to complete the rectification process , control points will be gathered to set it on the distorted image as a ground control points GCPs using different number of it , and using the different mathematical models to have the best accuracy of rectification.

1.3 Problem Statement

Because of the difficulties of having high resolution images in Gaza City, and the problem is commonly in developing countries, The research discussed the geometric rectification to have high resolution satellite images. So, the statement of the problem of our study summarized into two groups:

- The systematic distortions, and will be corrected by applying formulas derived by modeling the source of the distortions mathematically.

- The non-systematic (random) distortions and residual unknown systematic distortions and are corrected by analysis of the GCPs on the image.

After the previous corrections are applied, some of these images must be rectified to remove other types of distortions. So, applying rectification process is needed.

1.4 Research Aim and Objectives

The aim of this research is to study the two dimensional geometric rectification techniques for remote sensing satellite images of Gaza City as a case study due to the difficulties of having a high resolution and high accuracy satellite images in our study which in the developing countries commonly faces some problems such as , political , economical from funding to have these images and technical to have these images. So, our country is in need such as these images to use it at different fields.

To achieve this aim , the following objectives are to be determined :

- Study and analysis of the spatial accuracy that can be resulted in rectification process of Gaza City image.

- Study the best choice of mathematical models which gives the best accuracy.

2

- Study the effect of the GCPs number and the accuracy and what number of GCPs which will lead us to the best accuracy.

1.5 Methodology

To have the previous aim and objectives, there are many necessary steps should be followed to work this research as follows:

1) Literature review (previous studies).

2) Study the theory, the modeling of satellite geometry, the correction process, the fundamental and alternative mathematical models .

3) Experimental work and collecting data of Gaza City which include the images and GCPs.

4) Analyzing data using ERDAS Imagine software and the mathematical models to have a good accuracy of the rectification process.

5) Get conclusion and recommendations.

1.6 Research Structure

This research is oriented into five chapters and will be as followed :

Chapter 1 is the introduction of the research. In this chapter the problem and objectives of the research are explained and the methodology of the research will be explained.

Chapter 2 describes historic overview of remote sensing technology and its development stages. It also illustrates the basics of remote sensing and how it works with more details about each of these elements. This chapter also discusses the types and characteristics of satellite sensors as well as the most of the common image processing available in image analysis systems.

Chapter 3 gives the definition of the geometric correction process, then the fundamental and alternative mathematical models, then the rectification process is explained

Chapter 4 contains detailed description of the steps of the methodology of the research. It includes steps strategy beginning from data collection of imagery and image

processing of these images to use an existing of automatic feature extraction methods and methods evaluation.

Finally, Chapter 5 summarizes the conclusion outcomes and outlines the significant recommendations.

2 CHAPTER 2: REMOTE SENSING & DIGITAL IMAGE PROCESSING

2.1 Scope

This chapter describes historic overview of remote sensing technology and its development stages. It also illustrates the basic of remote sensing and how it works with more details about each of these elements. This chapter also discusses the types and characteristics of satellite sensors as well as the most common available image processing techniques used in image analysis systems.

2.2 Remote Sensing

There are many definitions for the remote sensing, but the famous definitions which can be summarize the remote sensing are two, the first defined the remote sensing as "the acquisition of information about an object or phenomenon without making physical contact with the object" . In modern usage, the term generally refers to the use of aerial sensor technologies to detect and classify objects on Earth (both on the surface, in the atmosphere and oceans) by means of propagated signals (e.g. electromagnetic radiation emitted from aircraft or satellites) (Aggarwal, 2003).

The second definition refers to the activities of recording, observing, and perceiving (sensing) objects or events in far-away (remote) places. Remote sensing refers to the science and technology of acquiring information about the earth's surface (i.e., land and ocean) and atmosphere using sensors onboard airborne (e.g., aircraft or balloons) or spaceborne (e.g., satellites and space shuttles) platforms (Weng, 2010).

2.2.1 Historic Overview

Satellite remote sensing can be traced to the early days of the space age (both Russian and American programs) and actually began as a dual approach to imaging surfaces using several types of sensors from spacecraft. In 1946, V-2 rockets acquired from Germany after World War II were launched to high altitudes from White Sands, New Mexico. These rockets, while never attaining orbit, contained automated still or movie cameras that took pictures as the vehicle ascended. Then, with the emergence of the

5

space program in the 1960s, Earth-orbiting cosmonauts and astronauts acted much like tourists by taking photos out the window of their spacecraft (Wikipedia, 2015).

The term "remote sensing," first used in the United States in the 1950s by Ms. Evelyn Pruitt of the U.S. Office of Naval Research, is now commonly used to describe the science of identifying, observing, and measuring an object without coming into direct contact with it. This process involves the detection and measurement of radiation of different wavelengths reflected or emitted from distant objects or materials, by which they may be identified and categorized by class/type, substance, and spatial distribution (Olsen, 2007).

Corona was America's first operational space-reconnaissance project. It was developed as a highly classified program under the joint management of the Central Intelligence Agency (CIA) and The United States Air Force (USAF), a relationship that evolved into the National Reconnaissance Office (NRO). For context, note that the first Soviet satellite, Sputnik, was launched on October 14, 1957, and Van Allen's Explorer spacecraft flew on a Redstone rocket on January 31, 1958. President Eisenhower approved the Corona program in February 1958. This proved to be farsighted, because when Francis Gary Powers was shot down in a U-2 on May 1, 1960, the president was forced to terminate reconnaissance flights over the Soviet Union (Olsen, 2007).

The first Corona test launch, on February 28, 1959, was the first of 12 failed missions in the Discover series (a cover name)—seven involving launch, five involving satellite and camera malfunctions. Mission 13 yielded the first successful capsule recovery from space on August 10, 1960. The first high-resolution images from space were taken on the next mission, August 18, 1960. The last Corona mission, number 145, was launched May 25, 1972; the last images were taken May 31, 1972 (Olsen, 2007).

Early imaging resolution was on the order of 8–10 m, eventually improving to 2 m (6 ft). Individual images on average covered approximately 10 miles by 120 miles. The system operated for nearly 12 years, and over 800,000 images were taken from space. The declassified image collection includes 2.1 million ft of film in 39,000 cans. The subsequent KH-7 mission acquired imagery with resolutions of 2–4 ft beginning in July 1963, with much smaller imaging areas. (Olsen, 2007)

6

Remote sensing systems continued to grow from the systems developed after the wars in the 1950s. Colour infrared (CIR) photography was discovered to be of great use for the plant sciences. In 1956, Colwell conducted experiments for the recognition and classification of vegetation types and the detection of damaged and diseased or stressed vegetation using of CIR. From 1950s up to now the significant progress in radar and sensing technology was achieved (Aggarwal, 2003).

Table 2.1 illustrate briefly the milestones in the history of remote sensing from the discovery of infrared to the high resolution systems, and at the science of remote sensing , the improvements are continuously.

Table 2.1: Milestones in the History of Remote Sensing

1800	Discovery of Infrared by Sir W. Herschel
1839	Beginning of Practice of Photography
1847	Infrared Spectrum Shown by J.B.L. Foucault
1859	Photography from Balloons
1873	Theory of Electromagnetic Spectrum by J.C. Maxwell
1909	Photography from Airplanes
1916	World War I: Aerial Reconnaissance
1935	Development of Radar in Germany
1940	WW II: Applications of Non-Visible Part of EMS
1950	Military Research and Development
1959	First Space Photograph of the Earth (Explorer-6)
1960	First TIROS Meteorological Satellite Launched
1970	Skylab Remote Sensing Observations from Space
1972	Launch Landsat-1 (ERTS-1) : MSS Sensor
1972	Rapid Advances in Digital Image Processing
1982	Launch of Landsat -4 : New Generation of Landsat Sensors: TM
1986	French Commercial Earth Observation Satellite SPOT
1986	Development Hyperspectral Sensors
1990	Development High Resolution Space borne Systems First Commercial Developments in Remote Sensing
1998	Towards Cheap One-Goal Satellite Missions
1999	Launch EOS : NASA Earth Observing Mission
1999	Launch of IKONOS, very high spatial resolution sensor system

7

2.2.2 Principles of Remote Sensing

The principles of remote sensing are based primarily on the properties of the electromagnetic spectrum and the geometry of airborne or satellite platforms relative to their targets.

Remote sensing is done by sensing and recording reflected or emitted energy and processing, analyzing, and applying that information. Our eyes are an excellent example of a remote sensing device. We are able to gather information about our surroundings by gauging the amount and nature of the reflectance of visible light energy from some external source (such as nature light as the sun or industry light bulb) as it reflects off objects in our field of view (CCRS, 2007).

The process of remote sensing involves an interaction between incident radiation and the targets of interest. This is exemplified by the use of imaging systems where the following seven elements are involved. Note, however that remote sensing also involves the sensing of emitted energy and the use of non-imaging sensors. Figure 2.1 shows the essential elements of a remote sensing system which included the following lines (CCRS, 2007):
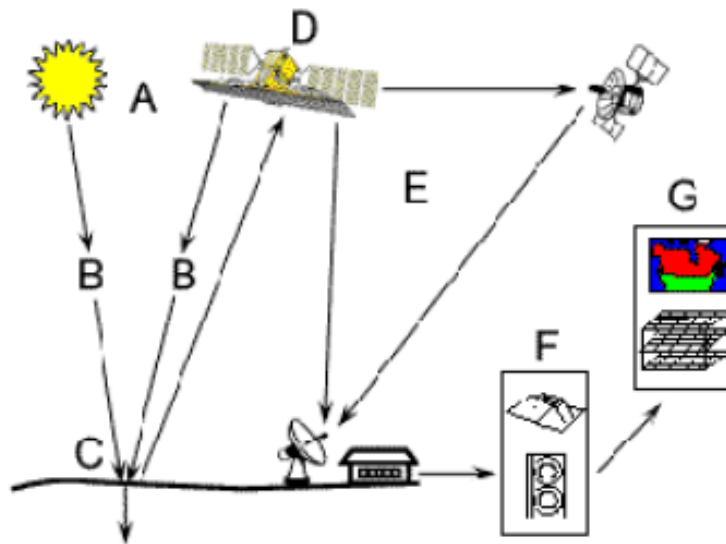
Figure 2.1: Elements of remote sensing system

8

- <u>Energy Source or Illumination (A)</u> - energy source which illuminates or provides electromagnetic energy to the target of interest consider the first requirement of remote sensing.

- <u>Radiation and the Atmosphere (B)</u> **-** as the energy travels from its source to the target, it will come in contact with and interact with the atmosphere it passes through. This interaction may take place a second time as the energy travels from the target to the sensor.

- <u>Interaction with the Target (C)</u> **-** after energy pass through atmosphere and reach the target; it interacts with the target depending on the properties of both the target and the radiation.

- <u>Recording of Energy by the Sensor (D)</u> **-** we require a sensor (remotely) to collect and record the electromagnetic radiation after the energy has been scattered by, or emitted from the target.

- <u>Transmission, Reception, and Processing (E)</u> **-** the energy recorded by the sensor has to be transmitted, often in electronic form, to a receiving and processing station where the data are processed into an image (hardcopy and/or digital).

- <u>Interpretation and Analysis (F)</u> **-** the processed image is interpreted, visually and/or digitally or electronically, to extract information about the target which was illuminated.

- <u>Application (G)</u> **-** after analyzing the raw information from images, the benefits achieved when we apply the information to better understand of issues and solving a particular problem in many fields.

2.2.3 Electromagnetic Radiation

Electromagnetic radiation consists of an electrical field which varies in magnitude, in a direction perpendicular to the direction in which the radiation is traveling, and a magnetic field oriented at right angles to the electrical field. Both these fields travel at the speed of light (C) as shown in Figure 2.2 (Sanderson, 2001).

9
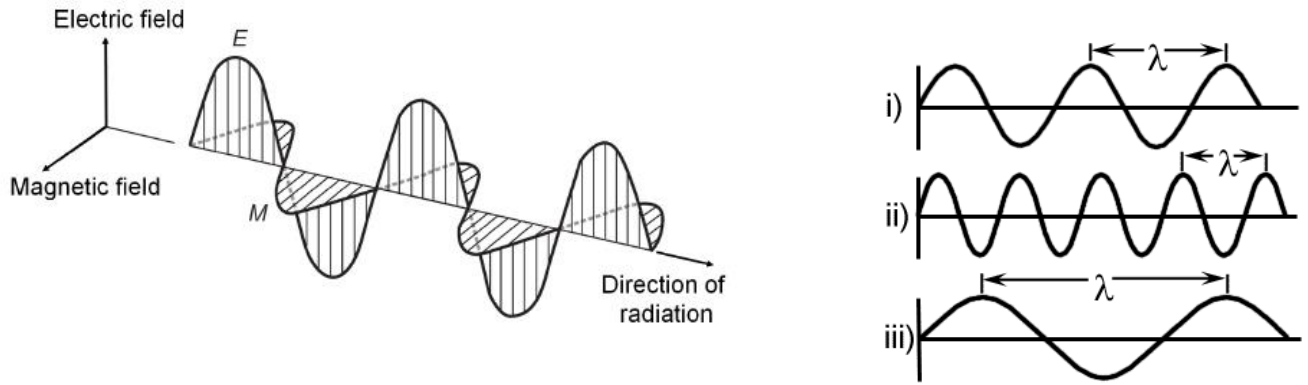
Figure 2.2: Electromagnetic radiation components

Two characteristics of electromagnetic radiation are particularly important for understanding remote sensing. These are the wavelength and frequency. The wavelength is the length of one wave cycle, which can be measured as the distance between successive wave crests. Wavelength is usually represented by the Greek letter lamda (λ). Wavelength is measured in meters (m) or some factor of meters such as nanometers (nm, 10^{-9} meters), micrometers (μm, 10^{-6} meters) or centimeters (cm, 10^{-2} meters). Frequency refers to the number of cycles of a wave passing a fixed point per unit of time. Frequency is usually represented by the Greek letter lambda (μ). Frequency is normally measured in hertz (Hz), equivalent to one cycle per second, and various multiples of hertz.

Wavelength and frequency are related by the following formula:

$$C = \lambda \times \mu \qquad \text{(Equation 2.1)}$$

Where C is speed of light (Weng, 2010).

2.2.4 Electromagnetic Spectrum

The electromagnetic Spectrum is defined as ranges from the shorter wavelengths (including gamma and x-rays) to the longer wavelengths (including microwaves and broadcast radio waves) between this ranges our eyes detect visible spectrum, which consist of three main colors **(RGB) (R**ed - **G**reen - **B**lue) from wavelengths approximately 0.4 to 0.7 μm. Moreover, there are several regions of the electromagnetic spectrum which are useful for some remote sensing applications as shown in Figure 2.3 (Aggarwal, 2003).

10
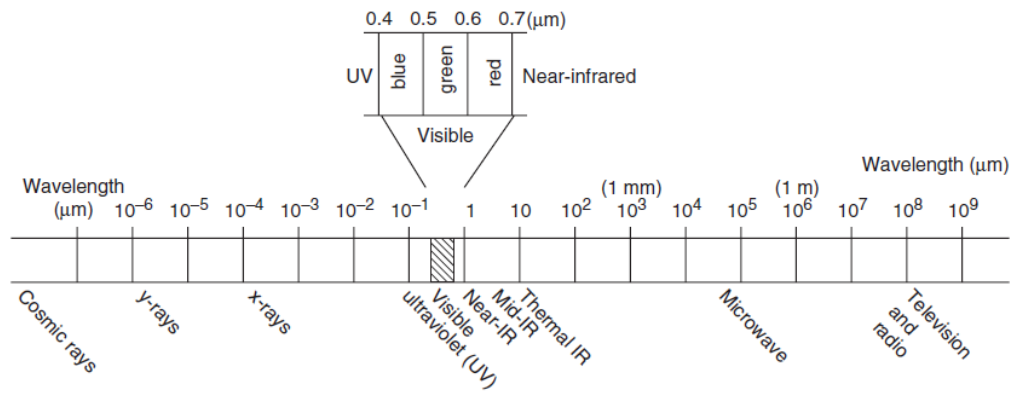
Figure 2.3: Electromagnetic spectrum components

The Electromagnetic spectrum is the continuum of energy ranging from kilometers to nanometers in wavelength. This continuum is commonly divided into the following ranges, called spectral bands, the boundaries between them being gradational (Levin, 1999).

Table 2.2 gives a description and some characteristics of different electromagnetic spectrum which started from Gamma rays to Radio waves.

Table 2.2: Principal Divisions of the Electromagnetic Spectrum

Wavelength	Description
Gamma rays <0.03 nm	Incoming radiation from the sun is completely absorbed by the upper atmosphere, and is not available for Remote Sensing.
X-rays 0.03 to 0.3 nm	Incoming radiation is completely absorbed by atmosphere. Not employed in Remote Sensing.
Ultraviolet (UV) region 0.30 μm - 0.38 μm ($1 \mu m = 10^{-6}$ m)	This region is beyond the violet portion of the visible wavelength. Material primarily rocks and minerals emit visible UV radiation. However UV radiation is largely scattered by earth's atmosphere and hence not used in field of remote sensing.

11

Wavelength	Description
Visible Spectrum 0.4 μm - 0.7 μm Violet 0.4 μm -0.446 μm Blue 0.446 μm -0.5 μm Green 0.5 μm - 0.578 μm Yellow 0.578 μm - 0.592 μm Orange 0.592 μm - 0.62 μm Red 0.62 μm - 0.7 μm	This is the light, which our eyes can detect. This is the only portion of the spectrum that can be associated with the concept of color. Blue Green and Red are the three primary colors of the visible spectrum. They are defined as such because no single primary color can be created from the other two, but all other colors can be formed by combining the three in various proportions. The color of an object is defined by the color of the light it reflects.
Infrared (IR) Spectrum 0.7 μm – 100 μm	Wavelengths longer than the red portion of the visible spectrum are designated as the infrared spectrum. British Astronomer William Herschel discovered this in 1800. The infrared region can be divided into two categories based on their radiation properties. Reflected IR (.7 μm - 3.0 μm) is used for remote sensing. Thermal IR (3 μm - 35 μm) is the radiation emitted from earth's surface in the form of heat and used for remote sensing.
Microwave Region 1 mm - 1 m	This is the longest wavelength used in remote sensing. The shortest wavelengths in this range have properties similar to thermal infrared region. The main advantage of this spectrum is its ability to penetrate through clouds.
Radio Waves (>1 m)	This is the longest portion of the spectrum mostly used for commercial broadcast and meteorology.

12

2.2.5   Sensors and Platforms

A sensor is a device that collect, measures and records energy reflected or emitted from a target or surface (electromagnetic energy). Platforms for remote sensors may be situated on the ground, on an aircraft or balloon (or some other platform within the Earth's atmosphere), or on a spacecraft or satellite outside of the Earth's atmosphere which is considered the famous platforms as shown in Figure 2.4 (Aggarwal, 2003).

Figure 2.4: Platforms for remote sensors

2.2.5.1   Type of Satellite Sensors

A sensor is a device that measures and records electromagnetic energy. Sensors can be divided into two types depending on energy resource:

1. Passive sensors depend on an external source of energy, usually the sun. Photographic camera is considered as passive sensor.

2. Active sensors have their own source of energy; an example would be a radar gun. These sensors send out a signal wave and measure the amount reflected back as shown in Figure 2.5 (Sanderson, 2001).

13
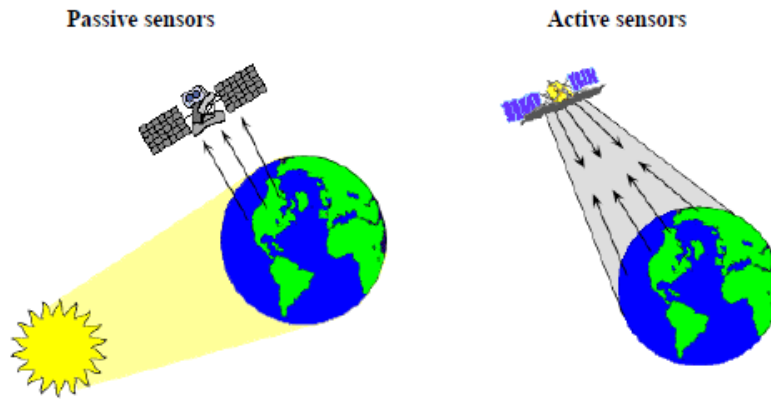
Figure 2.5: Type of satellites sensors

2.2.5.2 Satellite Sensor Characteristics

The principle of most satellite sensors is to gather information about the reflected radiation along a pathway, also known as the field of view **(FOV),** as the satellite orbits around the Earth. The smallest area of ground that is sampled is called the instantaneous field of view **(IFOV)**. The distance between the target being imaged and the sensor on platform, plays a great role in determining the detail of information obtained and the total area ground imaged by the sensor (Levin, 1999).

The IFOV is the angular cone of visibility of the sensor **(A)** and determines the area on the Earth's surface which is seen from a given altitude at one particular moment in time **(B)**. The size of the area viewed is determined by multiplying the IFOV by the distance from the ground to the sensor **(C)**. This area on the ground is called the resolution cell and determines a sensor's maximum spatial resolution (Levin, 1999).
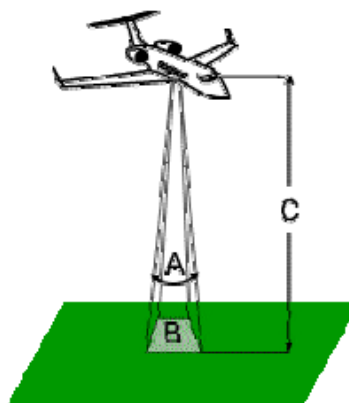
Figure 2.6: Instantaneous Field of View

14

The data collected by each satellite sensor can be described in terms of spatial, spectral, radiometric and temporal resolution (Sanderson, 2001).

- Spatial Resolution: The spatial resolution (known as ground resolution) refers to the size of the smallest possible feature that can be detected on ground by sensors, which depends primarily on their (IFOV), for example the spatial resolution or (IFOV) of Landsat Thematic Mapper ™ sensor is 30 m. So, the spatial resolution depends on image applications, some of satellites collect data at less than one meter spatial resolution but these are classified military satellites or very expensive commercial systems such as (IKONOS and OUIKBIRD satellites). Figure 2.7 shows an example at various spatial resolution (30, 5, 1) meter .
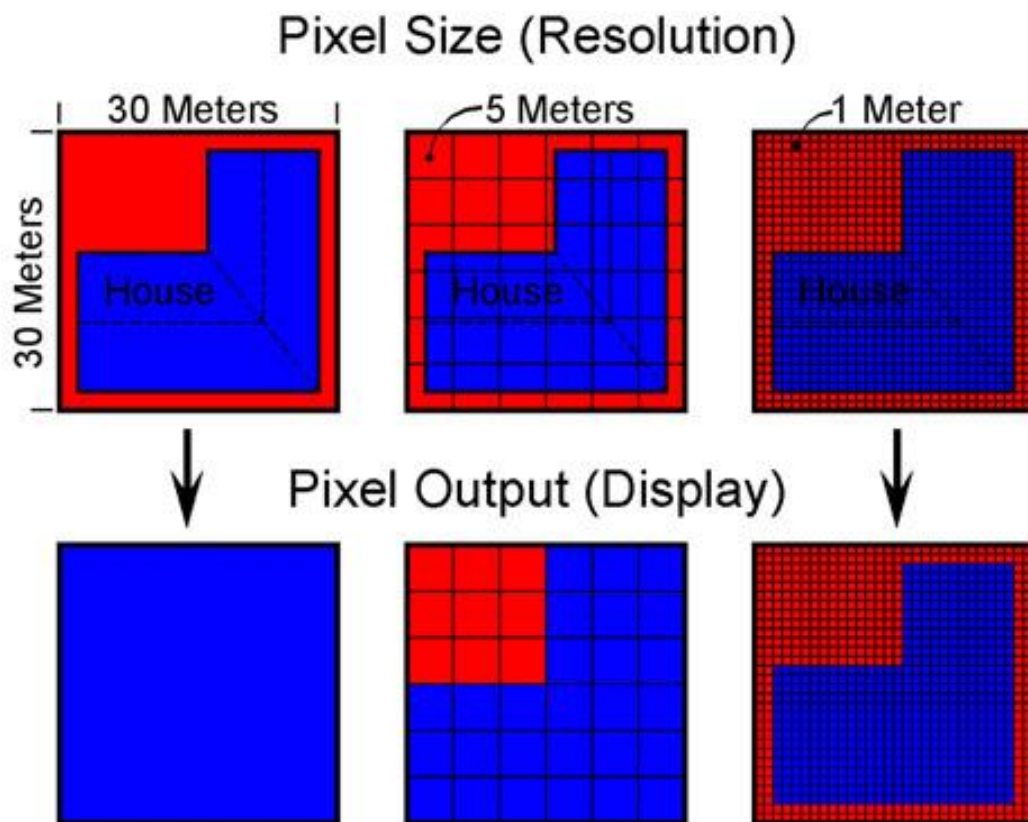
Figure 2.7: Spatial resolution

- Spectral Resolution: defined as the number and width of spectral bands in the sensing device, also describes the ability of a sensor to define fine wavelength

15

intervals. The simplest form of spectral resolution with one band (Sanderson, 2001).

- Radiometric Resolution: The radiometric resolution of an imaging system describes its ability to discriminate very slight differences in energy. The radiometric characteristics describe the actual information content in an image (CCRS, 2007).

- Temporal Resolution: Temporal resolution is very important in remote sensing system which refers to the length of time it takes for a satellite to complete one entire orbit cycle. The actual temporal resolution of a sensor depends on a variety of factors, including the satellite sensor capabilities, the swath overlap and latitude. With temporal resolution we are able to monitor changes that take place on the Earth's surface such as (urban development, floods, oil slicks, etc.) (Sanderson, 2001), for example Landsat 5 takes 16 day to complete one entire orbit cycle, Table 2.3 shows characteristics of various optical remote sensing systems (Levin, 1999).

Table 2.3 shows characteristics and illustrates more details of various optical remote sensing systems (Levin, 1999).

Table 2.3: Characteristics of various optical remote sensing systems

Satellite Sensor	Bands and wavelength (μm)	Spatial Resolution	Swath width	Repeat coverage	Orbit altitude (km)
NOAA	1 (0.58-0.68)	1.1 km	2399	daily	833
	2 (0.725-1.10)	1.1 km	2399	daily	833
	3 (3.55-3.93)	1.1 km	2399	daily	833
	4 (10.3-11.3)	1.1 km	2399	daily	833
	5 (11.5-12.5)	1.1 km	2399	daily	833
MSS 4-5	1 (0.5-0.6)	79/82m	185	16 days	705
	2 (0.6-0.7)	79/82m	185	16 days	705
	3 (0.7-0.8)	79/82m	185	16 days	705
	4 (0.8-1.1)	79/82m	185	16 days	705
TM 4-5	1 (0.45-0.52)	30m	185	16 days	705
	2 (0.52-0.60)	30m	185	16 days	705
	3 (0.63-0.69)	30m	185	16 days	705
	4 (0.76-0.90)	30m	185	16 days	705
	5 (1.55-1.75)	30m	185	16 days	705

16

Satellite Sensor	Bands and wavelength (μm)	Spatial Resolution	Swath width	Repeat coverage	Orbit altitude (km)
	6 (10.40-12.50)	120m	185	16 days	705
	7 (2.08-2.35)	30m	185	16 days	705
ETM 7	1 (0.45-0.515)	30m	183*170	16 days	705
	2 (0.525-0.605)	30m	183*170	16 days	705
	3 (0.63-0.69)	30m	183*170	16 days	705
	4 (0.75-0.90)	30m	183*170	16 days	705
	5 (1.55-1.75)	30m	183*170	16 days	705
	6 (10.40-12.5)	60m	183*170	16 days	705
	7 (2.09-2.35)	30m	183*170	16 days	705
	PAN (0.52-0.90)	15m	183*170	16 days	705
SPOT 4	XS 1 (0.50-0.59)	20m	60 (oblique scene at max 60 by 81)	26 days	822
	XS 2 (0.61-0.68)	20m	60 (oblique scene at max 60 by 81)	26 days	822
Satellite Sensor	Bands and wavelength (μm)	Spatial Resolution	Swath width	Repeat coverage	Orbit altitude (km)
	XS 3 (0.79-0.89)	20m	60 (oblique scene at max 60 by 81)	26 days	822
	XS 4 (1.58-1.75)	20m	60 (oblique scene at max 60 by 81)	26 days	822
	Monospectral red (0.61-0.68)	10m	60 (oblique scene at max 60 by 81)	26 days	822
IRS 1C	LISS 1 (0.52-0.59)	23.6m	142	24 days	818
	LISS 2 (0.62-0.68)	23.6m	142	24 days	818
	LISS 3 (0.77-0.86)	23.6m	142	24 days	818
	LISS 4 (1.55-1.70)	70.8m	148	24 days	818
	WIFS 1 (0.62-0.68)	189m	810	24 days	818
	WIFS 2 (0.77-0.86)	189m	810	24 days	818
	PAN (0.5-0.75)	5.8m	70	24 days	818
IKONOS	Multispectral (0.45-0.52)	4m	13 at nadir	2.9 days 1m resolution	681

17

Satellite Sensor	Bands and wavelength (μm)	Spatial Resolution	Swath width	Repeat coverage	Orbit altitude (km)
	Multispectral (0.52-0.60)	4m	13 at nadir	2.9 days 1m resolution	681
	Multispectral (0.63-0.69)	4m	13 at nadir	2.9 days 1m resolution	681
	Multispectral (0.76-0.90)	4m	13 at nadir	2.9 days 1m resolution	681
	Panchromatic (0.45-0.90)	1m	13 at nadir	2.9 days 1m resolution	681

18

3 CHAPTER 3: LITERATURE REVIEW

3.1 Scope

This chapter gives a background of rectification processing of remote sensing images. This chapter firstly reviews the previous studies, source of geometric distortions, compares the different mathematical models being currently used for the geometric distortion modeling, details the algorithms, methods and processing steps and finally tracks the error propagation from the input to the final output data .

3.2 Review of Geometric Correction

The rectification operations of digital images is important operations that applied on the satellite images to eliminate several types of geometric distortions and enhancing the satellite image resolution and accuracy.

Consequently , many researchers and studies were performed to dial with this important problem from.

Guoqing Zhou and Ron Li discussed the mathematical model of the bundle adjustment and the experimental results on the attainable accuracy of ground points versus number and distribution of ground control points. The image measurement error of ground control and check points versus the order of the polynomial fit to the orbital path also studied. The test area was Madison Country in central Ohio, which IKONOS imagery was simulated about this area. It was found that four or more ground control points are recommended for computing high accurate ground points and reducing costs, the distribution of ground control points along a straight line will not increase the accuracy of ground points, a well spread distribution even few GCPs is more beneficial to accuracy improvement than a dense poorly spread distribution, ground accuracy , the higher precision position and attitude data will improve the geometric accuracy of ground points (Zhou and Li, 2000).

A strict geometric model based on affine transformation was proposed by Jianqing Zhang and Zuxun Zhang to solve the traditional parameters (position and orientation) of high resolution satellite images. This model adopted new method with three steps. These steps were based on parallel ray projection. The first one was the reducing of the

three dimensional space to the image space by the similar transformation. In the second step, the resulted space was projected to the level plane that passes from the center of the image plane, by the parallel rays (affine transformation). In the third step, the level image is transformed to the original declining image. By this method, the problem of the relativity of image parameter calculation was solved completely . The validity of the strict geometric model had been verified by some experiments, these experiments carried on images with 10,3 and 1-meters resolution (Zhang, 2000).

M.J Valadan Zoej, A. Mansourian, B Mojaradi, S. Sadeghian discussed the mathematical solution to extract planimetric information as accurate as possible from IKONOS images. They used in their study genetic algorithm technique to find the Best terms of global polynomial that provides the best fitness model of the imagery to the ground space, then by using the output of the global polynomial in multiquadric transformation the results were the best in the term of accuracy. The test area in Hamedan city in Iran (Zoej et al., 2002).

Fast geometric rectification method for space-borne SAR (Synthetic Aperture Radar) digital image with no ground control point was studied by Caiying ZHU, Guowarg ,JIN and Qifig XU, The Fast geometric rectification method introduced in this study was based on the study of SAR imaging principle and the law of geometric distortion in slant range image. The results of the experiment indicated that the time spent in the fast geometric rectification is only one tenth of that spent in the digital differential rectification and their precision was almost equal (ZHU et al.,2002).

The geometric correction process of IKONOS satellite imagery was studied by Hala - H. Amin by using the non-parametric approach. This study contained the evaluating of the effect number and distribution of GCPs, also the source of GCPs was evaluated, from GPS or from the map. Amin found that the same results can be reached by using 5 GCPs form GPS and 7 GCPs from the map and these are the suitable results. These results are; by using GPS measurements can be reached 0.8 to 0.11 m, and by using the map measurements the average is 6m and the maximum is 8m (Amin, 2004).

F. Eltohamy and E. H. Hamza studied the effect of ground control points location and distribution on geometric correction accuracy of remote sensing satellite images and

20

have a results which can be summarized in three points , the first point that the bad location and bad distribution of the selected GCPs lead to increase in the average RMS error value of correction of an image .Second point says that the effect of bad location of selected GCPs is more severe than that of bad distribution of selected GCPs on the correction accuracy. Finally the third points explain that to obtain high accuracy of geometric correction of remote sensing satellite images, the location and distribution of selected GCPs should be taken into consideration as mentioned before (Eltohamy and Hamza, 2009).

Partial distortion correction of remote sensing image rectification error was studied by Feng Wang , he explained that the rectification error existing in rectified image is a common problem and this error existing in partial area distributes irregularly. At present, remote sensing image processing software both in China and abroad all focus on rectification of image using mathematical equation generated from control points and ignores partial distortion. This paper have done preliminary research on partial distortion rectification based on overlaying digital raster graphics and remote sensing image to discover distortion error visually. In preliminary research, this paper obtains good results using simplified algorithm. Further research will be focused on overlaying image with image having different time phase, different remote sensing source and distortion rectification inside arbitrary polygon (Wang, 2001).

A paper prepared by Narayan Panigrahi, B.K. Mohan and G. Athithan discussed the pre-processing algorithm for rectification of geometric distortions in satellite images in the paper, a pre-processing algorithm has been proposed which removes systematic distortions of a satellite image and thereby removes the blank portion of the image. It is an input to output mapping of image pixels, where the transformation computes the coordinate of each output pixel corresponding to the input pixel of an image. The transformation is established by the exact amount of scaling, rotation and translation needed for each pixel in the input image so that the distortion induced during the recording stage is corrected(Panigrahi, et .al, 2011).

Development in geometric modeling for high resolution satellite pushbroom sensors is discussed by Daniela Poli and Thierry Toutin, their paper seeks to report the main characteristics and developments of optical pushbroom sensors for photogrammetric

21

and remote sensing applications, and to provide a critical review of approaches used for their geometric modeling (Poli and Toutin, 2012).

Capt. Dr. S. Santhosh Baboo & Mr. S. Thirunavukkarasu discussed geometric correction in high resolution satellite imagery using mathematical methods with a case study in Kiliyar Sub Basin and conclude the study with the results of practical test that hybrid model gives the best results compared to the mathematical methods especially for high resolution satellite imageries such as IRS-P6 Liss III. The main advantages of this model are increased accuracy, simple calculations and lesser number of ground control points required. Future research work may be selecting effective ground control points in point wise polynomial functions utilizing projective transformation(Baboo and Thirunavukkarasu, 2014) .

A. L. Choo, Y. K. Chan, and V. C. Koo studied the process of the geometric correction on SAR Imagery. In the process of geometric correction, the selection of GCPs is very important as it will generated the mathematical distortion model that will relate the distorted image and the reference image. The resampling of the image will produces a better quality image (Choo, et.al.2012).

A.Al Yossof studied the two dimensional geometric rectification on QuickBird satellite image and found that the second order polynomial model gives the highest spatial accuracy in the rectification process with accuracy of the rectification process can be from one and half to two pixels, also he found that with QuickBird standard image, and the rectification process, 8 control points for each direction (X and Y) are enough to get spatial accuracy from one and half to two pixels (Al Yossef, 2004).

Yang Guang and Jiao Weili discussed the Impact of GCPs distribution on image geometric rectification, after some existing methods about automatic optimization of GCP are summarized, a new method of automatic optimization of GCPs based on Voronoi Diagram (Thiessen polygon) is proposed. This method uses the ratio of Thiessen Polygon max-min area generated by GCPs as the basis and filter GCPs from the overfull ones without manual subjectivity for better accuracy. Experiments in this paper also demonstrated the relationship between the accuracy of geometric correction and the distribution of GCPs (Guang and Weili, 2011) .

22

Minakshi Kumar explained the digital image processing of satellite data which can be primarily grouped into three categories: Image Rectification and Restoration, Enhancement and Information extraction. Image rectification is the pre-processing of satellite data for geometric and radiometric connections. Enhancement is applied to image data in order to effectively display data for subsequent visual interpretation. Information extraction is based on digital classification and is used for generating digital thematic map (Kumar, 2003).

A Case Study in Coimbatore, Tamil Nadu was studied by Baboo and Devi about geometric correction in recent high resolution satellite imagery. The paper shows that the geometric correction process done in the Coimbatore imagery to improve the quality, and it shows the process of distortion removed .Finally they get the georectified image using ERDAS Imagine 9.1 (Baboo and Devi, 2011).

3.3   Types of Distortions

Raw data of the image usually have many distortions which divided into two types of distortions depending on the reason of it and categorized to geometric and random distortions as follows :

3.3.1   Geometric Distortions

Geometric distortion is an error on the satellite image between the actual image coordinates and the ideal image coordinates. It's a principle reason of our inaccurate measurements, and these distortions divided into two types of distortions which are systematic and non- systematic distortions as follows:

3.3.1.1   Systematic Distortions

Systematic distortion occurs when coordinates are consistently off by a certain amount across the whole image. Systematic distortion is caused by factors that vary in a consistent manner. Cartographers, for example, have been concerned for centuries with the systematic distortion that occurs when one attempts to portray a sphere (the earth) as a flat surface (the map), which has led to many differing projection approaches. In addition, remote sensors worry about systematic distortions associated with the platform motion and imaging device. For example, the rate at which the earth rotates out from

23

beneath a satellite cause systematic distortion, as does the rate at which off-nadir scale changes across an image (ELtohamy and Hamza, 2009).

Systematic distortions can be corrected by applying formulas derived by modeling the sources of the distortions mathematically and use these models to establish correction formulae. These modeling techniques require prior knowledge about the orbit parameters; the nature and the magnitude of the sources of distortion during the scene acquisition time. Sometimes this prior information is not available and consequently these techniques cannot be applied (ELtohamy and Hamza, 2009).

Some reasons which occurs the systematic distortions listed as follows (ELtohamy and Hamza, 2009):

- Scan Skew: Caused by the forward motion if the platform during the time required for each mirror sweep. The ground swath is not normal to the ground track but is slightly skewed, producing cross-scan geometric distortion.

- Mirror Scan Velocity Variance: The mirror scanning rate is usually not constant across a given scan, producing along-scan geometric distortion.

- Panoramic Distortion: The ground area imaged is proportional to the tangent of the scan angle rather than to the angle itself. Because data are sampled at regular intervals, this produces along-scan distortion.

- Platform Velocity: If the speed of the platform changes, the ground track covered by successive mirror scans changes, producing along-track scale distortion.

- Earth Rotation: Earth rotates as the sensor scans the terrain. This results in a shift of the ground swath being scanned, causing along-scan distortion.

Systematic distortions are well understood and corrected by applying formulas derived by modeling the sources of the distortions mathematically. For example, a highly systematic source of distortion involved in multispectral scanning from satellite altitudes is the eastward rotation of the earth beneath the satellite during imaging. This causes each optical sweep of the scanner to cover an area slightly to the west of the

24

previous sweep. This is known as skew distortion. The process of deskewing the resulting imagery involves offsetting each successive scan line slightly to the west. The skewed parallelogram appearance of satellite multispectral scanner data is a result of this correction (Remote Sensing Notes, 1999).

(a) Radial distortion   (b) Tegential distortion   (c) Scale error   (d) Projection distortion

(e) Skew   (f) Along track scale error   (g) Step-wise distortion   (h) Scan-line scale error
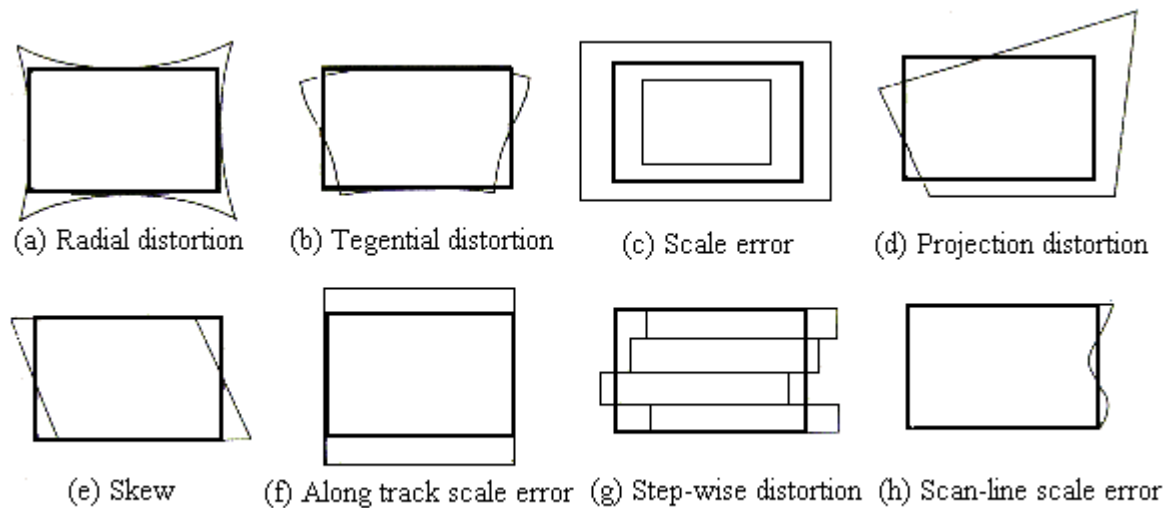
Figure 3.1 Systematic distortion

3.3.1.2   Non-systematic (random / unpredictable) distortions

Nonsystematic distortion is another broad category of image distortion. Nonsystematic distortion occur when random factors cause local variations in image scale and coordinate location. Nonsystematic distortion is particularly common in airborne imagery, where turbulence and variations in ground topography can alter the image scale over short distances. Likewise, the direction in which the sensor is pointed varies with the pitch, yaw and role of the aircraft, which in turns causes the coordinates of the pixels' locations to change in a nonsystematic manner. Nonsystematic distortion can be so severe at times that the same pixel may be resampled multiple times, or some locations on the ground may be entirely missed. Figure 3.2 represents a classic case of nonsystematic image distortion due to pitch, yaw and roll of the helicopter that was carrying the sensor (resolution is ~1-m) (ELtohamy and Hamza, 2009).

25

Nonsystematic distortion corrected through the use of ground control points (GCP's) with the used mathematical method.

Some reasons which occurs the nonsystematic distortion listed as following (Remote Sensing Notes, 1999):

- Altitude Variance: If the sensor platform departs from its normal altitude or the terrain increases in elevation, this produces changes in scale or pixel size.

- Platform Attitude: One sensor system axis is usually maintained normal to Earth's surface and the other parallel to the spacecraft's direction of travel. If the sensor departs form this attitude, geometric distortion results.

Random distortions and residual unknown systematic distortions are corrected by analyzing well-distributed ground control points (GCPs) occurring in an image. As with their counterparts on aerial photographs, GCPs are features of known ground location that can be accurately located on the digital imagery. Some features that might make good control points are highway intersections and distinct shoreline features. In the correction process numerous GCPs are located both in terms of their two image coordinates (column, row numbers) on the distorted image and in terms of their ground coordinates (typically measured from a map, or GPS located in the field, in terms of UTM coordinates or latitude and longitude) (Remote Sensing Notes, 1999).
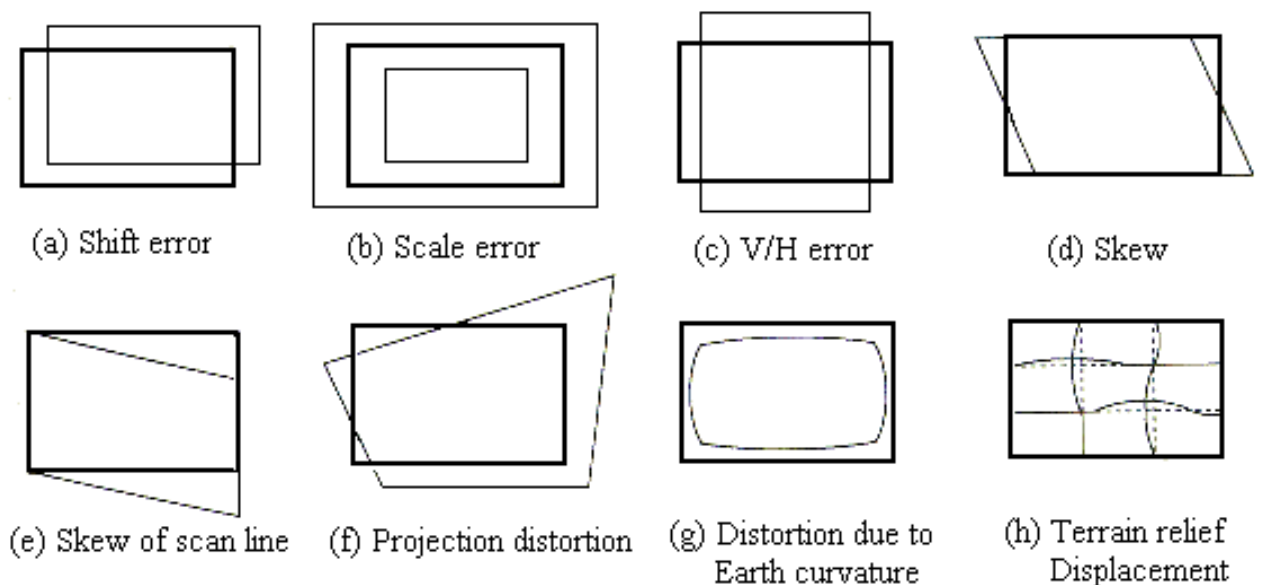

(a) Shift error   (b) Scale error   (c) V/H error   (d) Skew

(e) Skew of scan line   (f) Projection distortion   (g) Distortion due to Earth curvature   (h) Terrain relief Displacement

Figure 3.2 Nonsystematic distortion

27

3.3.1.3   Radiometric Correction

As any image involves radiometric errors as well as geometric errors, these errors should be corrected. Radiometric correction is to avoid radiometric errors or distortions, while geometric correction is to remove geometric distortion.

When the emitted or reflected electro-magnetic energy is observed by a sensor on board an aircraft or spacecraft, the observed energy does not coincide with the energy emitted or reflected from the same object observed from a short distance. This is due to the sun's azimuth and elevation, atmospheric conditions such as fog or aerosols, sensor's response etc. which influence the observed energy. Therefore, in order to obtain the real irradiance or reflectance, those radiometric distortions must be corrected. Radiometric correction is classified into the following three types (see Figure 3.3)
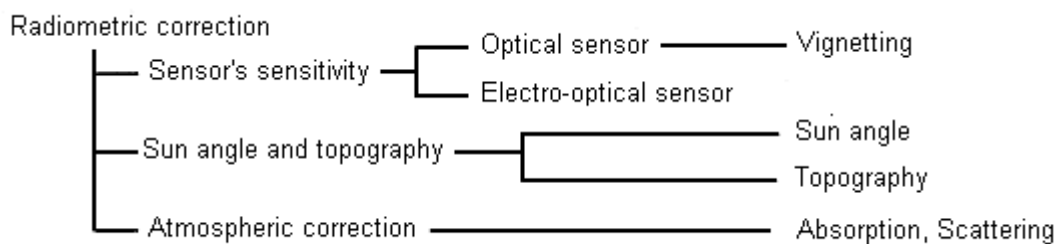
Figure 3.3 Radiometric Correction

(1) Radiometric correction of effects due to sensor sensitivity In the case of optical sensors, with the use of a lens, a fringe area in the corners will be darker as compared with the central area. This is called vignetting. Vignetting can be expressed by $\cos^n\theta$, where θ is the angle of a ray with respect to the optical axis. n is dependent on the lens characteristics, though n is usually taken as 4. In the case of electro-optical sensors, measured calibration data between irradiance and the sensor output signal, can be used for radiometric correction.

(2) Radiometric correction for sun angle and topography.

- Sun Spot : The solar radiation will be reflected diffusely onto the ground surface, which results in lighter areas in an image. It is called a sun spot. The sun spot together with vignetting effects can be corrected by estimating a shading

28

curve which is determined by Fourier analysis to extract a low frequency component .

- Shading : The shading effect due to topographic relief can be corrected using the angle between the solar radiation direction and the normal vector to the ground surface.

(3) Atmospheric correction : Various atmospheric effects cause absorption and scattering of the solar radiation. Reflected or emitted radiation from an object and path radiance (atmospheric scattering) should be corrected for (see Figure 3.4) (Remote Sensing Notes, 1999).
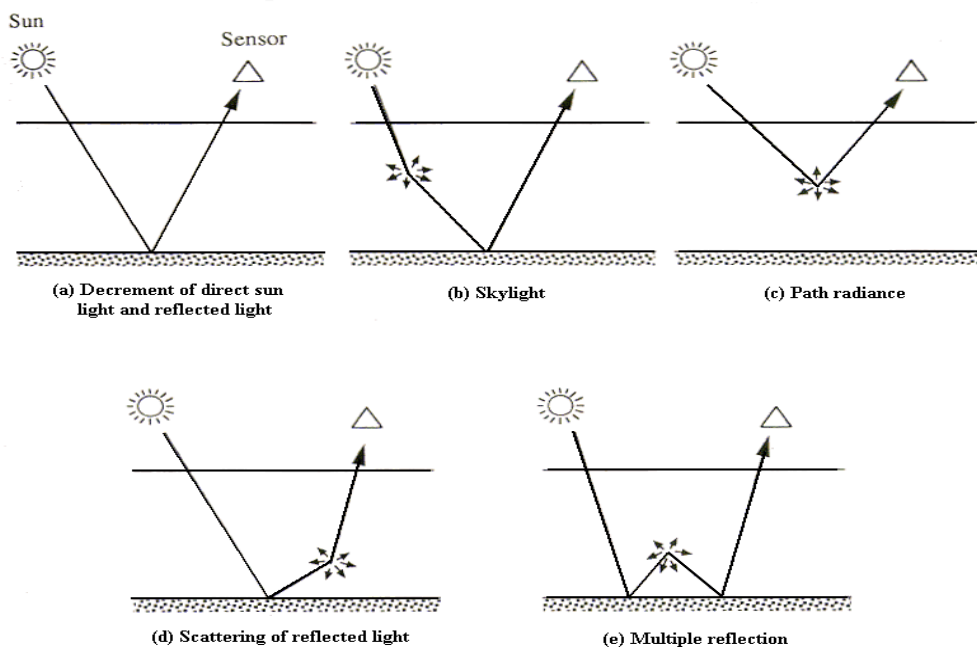
Figure 3.4 Atmospheric correction

3.4 Satellite Images Mathematical Models

3.4.1 Fundamental Mathematical models of Satellite Imagery

3.4.1.1 Modified Collinearity Equations

The well known collinearity equations, which provide the fundamental mathematical model for restitution of photogrammetric frame imagery, are equally applicable to satellite line scanner imagery, though in modified form. The modified model takes into account the fact that the line scanner represents a perspective projection in the cross-track direction (y) only, and a parallel projection in the x, or flight-line direction. This yields the following equations related to a particular scan line at time t:

$$0 - x_0 = -cX^1/Z^1 \qquad \text{Equation (3.1)}$$

$$y_t - y_0 = -cY^1/Z^1 \qquad \text{Equation (3.2)}$$

And

$$(X^1, Y^1, Z^1)^T = R_t \left[(X - X_t^c), (Y - Y_t^c), (Z - Z_t^c) \right]^T \qquad \text{Equation (3.3)}$$

where is y_t the image coordinate within the scan line (the x coordinate is zero); x_0 , y_0 are the coordinates of the principal point; c is the principal distance; X, Y, Z are the coordinates of the ground point; X_t^c, Y_t^c , Z_t^c are the object space coordinates of the sensor at time t; and R_t is the sensor orientation matrix, again at time t. In order to perform exterior orientation (EO) and subsequent ground point triangulation using Eqs. 1, it is necessary to model the orientation parameters (R_t, X_t^c, Y_t^c , Z_t^c) as a function of time, otherwise the model is too over-parameterized to support practical implementation. The modeling of the sensor platform dynamics as a function of time or scan-line number is less problematic for spaceborne sensors than for airborne linear array scanners due to the relatively smooth and quite well described orbital trajectory of the satellite, (Fraser, 2000) .

30

3.4.1.2   Bundle Adjustment Formulation

In the case where the orbital parameters of the satellite are known a priori, the positional elements of the EO can be constrained to some degree. This incorporation of prior knowledge regarding satellite motion can range from the simple assumption that the EO parameters vary either linearly or as a quadratic function over a short arc length, to the case where R_t and X_t^c, Y_t^c , Z_t^c are accurately known through the use of on-board GPS and star trackers which determine sensor attitude angles. A common approach, lying somewhere between these two, is to enforce the platform motion to be in accordance with a true Keplerian orbital trajectory. Thus, the 'shape' of the trajectory is assumed known a priori, but not the position. With these considerations in mind, a combined mathematical model for satellite line scanner imagery can be written as:

$$v = A_1 x_1 + A_2 x_2 + A_3 x_3 - l : P$$

Equation (3.4)

$$v_c = C_1 x_1 + C_3 x_3 - l_c : P_c$$

Equation (3.5)

where x_1, x_2 and x_3 represent the EO, object point and additional parameters, respectively; A_1, A_2 and A_3 are the related design matrices; C_1 and C_3 are coefficient matrices of orbital constraint functions; v and v_c are vectors of residuals; l and l_c are discrepancy vectors; and P and P_c are weight matrices , (Fraser, 2000).

3.4.2   The Alternative Mathematical Models

3.4.2.1   Two Dimensional Polynomial Models

Polynomial models usually can be used in the transformation between image coordinates and object coordinates. The needed transformation can be expressed in different orders of the polynomials based on the distortion of the image, the number of GCPs and terrain type. The 1st order transformation is a linear transformation, which can change location , scale, skew, and rotation. In most cases, first order polynomial used to project raw imagery to a object for data covering small areas . Transformations of the 2nd-order or higher are nonlinear transformations that can be used to convert

31

Lat/Long data to object or correct nonlinear distortions such as Earth curvature, camera lens distortion. The following equations are used to express the general form of the polynomial models in 2D and 3D cases :

Two-dimensional general polynomials

- The First order polynomials

$$x = a_0 + a_1 X + a_2 Y \qquad \text{Equation (3.6)}$$

$$y = b_0 + b_1 X + b_2 Y \qquad \text{Equation (3.7)}$$

- The Second order polynomials

$$x = a_0 + a_1 X + a_2 Y + a_3 XY + a_4 X^2 + a_5 Y^2 \qquad \text{Equation (3.8)}$$

$$y = b_0 + b_1 X + b_2 Y + b_3 XY + b_4 X^2 + b_5 Y^2 \qquad \text{Equation (3.9)}$$

- The Third order polynomials

$$x = a_0 + a_1 X + a_2 Y + a_3 XY + a_4 X^2 + a_5 Y^2 + a_6 X^2 Y + a_7 XY^2 + a_8 X^3 + a_9 Y^3 \qquad \text{Equation (3.10)}$$

$$y = b_0 + b_1 X + b_2 Y + b_3 XY + b_4 X^2 + b_5 Y^2 + b_6 X^2 Y + b_7 XY^2 + b_8 X^3 + b_9 Y^3 \qquad \text{Equation (3.11)}$$

- Two dimensional general polynomials

$$x = \sum_{i=0}^{m} \sum_{j=0}^{m} a_{ij} X^i Y^j \qquad \text{Equation (3.12)}$$

$$y = \sum_{i=0}^{m} \sum_{j=0}^{m} b_{ij} X^i Y^j \qquad \text{Equation (3.13)}$$

where (a,b) are the model coefficients, (X,Y) are model parameters (Amini and Hashemi, 2005).

3.4.2.2 The Projective Model

Projective model express the relationship between two space based on perspective projection concepts. The basic elements of the perspective projection consist of the point of the perspective center, bundle of arrays through this point and two different

32

planes cut the bundle of arrays and do not contain perspective center. These two space can be defined in our work as image space and the ground space.The relationship between the two spaces can be written the following formula, Eight-parameter transformation model :

$$x = \frac{L_0 + L_1 X + L_2 Y}{1 + L_6 X + L_7 Y}$$

Equation (3.14)

$$y = \frac{L_3 + L_4 X + L_5 Y}{1 + L_6 X + L_7 Y}$$

Equation (3.15)

where L is the model coefficient, (x, y) are the image coordinates and (X ,Y) are the terrain coordinates (Amini and Hashemi , 2005).

3.4.2.3   The Affine Model

Adoption of an affine model as opposed to perspective projection model for satellite line scanner imagery has been previously considered for both SPOT and MOMS-02 imagery and results showed that the affine model is quite robust and stable for image orientation and triangulation. The noteworthy point is that using the affine model can save at least thirty percent on image prices by ordering stereo images without the need for the rational functions.

Each observation of a GCP will give rise to a set of two affine condition equations derived from the relationship between the image coordinates and the GCP coordinates in the geocentric system. The two affine condition equations are as follows :

In 3D

$$x = a_0 + a_1 X + a_2 Y + a_3 Z$$

Equation (3.16)

$$y = b_0 + b_1 X + b_2 Y + b_3 Z$$

Equation (3.17)

In 2D

$$x = a_0 + a_1 X + a_2 Y$$

Equation (3.18)

33

$$y = b_0 + b_1 X + b_2 Y \qquad \text{Equation (3.19)}$$

Where (x, y ,z) are the image coordinates and (X, Y, Z) are the ground coordinates(Amini and Hashemi , 2005).

3.4.2.4 Helmert Transformation

Helmert transformation describes the transformation between the image system and the ground coordinate system as the equation :

$$x = \begin{bmatrix} X \\ Y \end{bmatrix} = S * \begin{bmatrix} \cos\theta & -\sin\theta \\ \sin\theta & \cos\theta \end{bmatrix} * \begin{bmatrix} x \\ y \end{bmatrix} + \begin{bmatrix} \Delta x \\ \Delta y \end{bmatrix} \qquad \text{Equation (3.20)}$$

Where X and Y are the object point coordinates , x and y are the image coordinates S is the scale factor between the two systems and θ is the rotation angel between the two systems. (Spath, 2004).

3.4.2.5 Rational Functions

As a practical means of extracting 3D information from stereo satellite imagery in the absence of either a camera model or EO data, a model based on 'rational functions' has been proposed. Rational functions are polynomial-based, empirical models which generally comprise terms to third order and express image coordinates as a direct function of object space coordinates, in much the same way as do collinearity equations. These functions, which provide a continuous mapping between image and object space, are given as a ratio of polynomials comprising coefficients that defy straightforward geometric interpretation. Indeed, it is said that one reason rational functions gained popularity for military imaging satellites was that the satellite orbital elements and also the EO could not be derived from the rational function coefficients.

A general model for the rational function approach, which is appropriate for mono and stereo imaging configurations, is given as:

$$x_t = \frac{a_0 + a_1 X + a_2 Y + a_3 Z + a_4 XY + a_5 XZ + a_6 YZ + a_7 XYZ + a_8 X^2 + \ldots\ldots + a_{19} Z^3}{1 + b_1 X + b_2 Y + b_3 Z + b_4 XY + b_5 XZ + b_6 YZ + b_7 XYZ + b_8 X^2 + \ldots\ldots + b_{19} Z^3} \quad \text{Equation (3.21)}$$

$$y_t = \frac{c_0 + c_1 X + c_2 Y + c_3 Z + c_4 XY + c_5 XZ + c_6 YZ + c_7 XYZ + c_8 X^2 + \ldots\ldots + c_{19} Z^3}{1 + d_1 X + d_2 Y + d_3 Z + d_4 XY + d_5 XZ + d_6 YZ + d_7 XYZ + d_8 X^2 + \ldots\ldots + d_{19} Z^3} \quad \text{Equation (3.21)}$$

34

Where x_t, y_t are the image coordinates and X,Y,Z the object point coordinates and a_0 to $a19$, b_1 to b_{19}, c_0 to c_{19} and d_1 to d_{19} are the Rational Polynomial Coefficients RPC.

The advantage of different types of images can be done with the same software by changing the polynomial's coefficients for different types of sensors (Fraser , 2000).

3.4.2.6   Direct Linear Transformation DLT

The DLT models the transformation between the image pixel coordinate system and the object space coordinate system as a linear function . This model has been widely used in close range photogrammetry and the model is often used to derive the approximate initial values of the unknown parameters for the collinearity equations. DLT has three additional unknowns when compared to the projective Transformation:

$$x = \frac{a_1 X + a_2 Y + a_3 Z + a_4}{1 + c_1 X + c_2 Y + c_3 Z} \qquad \text{Equation (3.22)}$$

$$y = \frac{b_1 X + b_2 Y + b_3 Z + b_4}{1 + c_1 X + c_2 Y + c_3 Z} \qquad \text{Equation (3.23)}$$

Where x, y are the image coordinates and X,Y,Z the object point coordinates and a_1, a_2, a_3, a_4, b_1, b_2, b_3, b_4, c_1, c_2, and c_3 are the linear orientation parameters between two dimensional image space and three dimensional object space (Ok and Turker, 2005).

3.5 Root Mean Square Error

RMS error is the distance between the input (source) location of a GCP and the retransformed location for the same GCP. In other words, it is the difference between the desired output coordinate for a GCP and the actual output coordinate for the same point, when the point is transformed with the geometric transformation (Intergraph Corporation, 2013).

RMS error is calculated with a distance equation:

35

$$\text{RMS error} = \sqrt{(x_r - x_i)^2 + (y_r - y_i)^2}$$

Equation (3.24)

Where:

x_i and y_i are the input source coordinates

x_r and y_r are the retransformed coordinates

RMS error is expressed as a distance in the source coordinate system. If data file coordinates are the source coordinates, then the RMS error is a distance in pixel widths. For example, an RMS error of 2 means that the reference pixel is 2 pixels away from the retransformed pixel (Intergraph Corporation, 2013).

3.5.1 Residuals and RMS Error Per GCP

Residuals are the distances between the source and retransformed coordinates in one direction. The X residual is the distance between the source X coordinate and the retransformed X coordinate. The Y residual is the distance between the source Y coordinate and the retransformed Y coordinate (Intergraph Corporation, 2013).

If the GCPs are consistently off in either the X or the Y direction, more points should be added in that direction.

3.5.2 Root Mean Square Error Per GCP

The RMS error of each point is reported to help you evaluate the GCPs. This is calculated with a distance formula (Intergraph Corporation, 2013):

$$R_i = \sqrt{XR_i^2 + YR_i^2}$$

Equation (3.25)

Where:

R_i = RMS error for GCP$_i$

XR_i = X residual for GCP$_i$

YRi = Y residual for GCP$_i$

36

Figure 3.5 illustrates the relationship between the residuals and the RMS error per point.
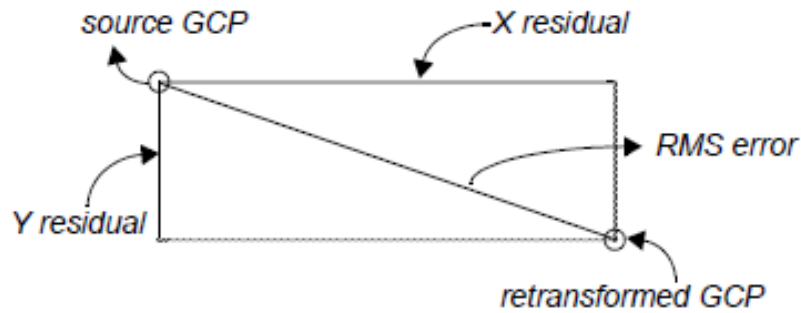
Figure 3.5 Residuals and RMS Error Per Point

3.5.3   Total Root Mean Square Error

From the residuals, the following calculations are made to determine the total RMS error, the X RMS error, and the Y RMS error (Intergraph Corporation, 2013):

$$R_x = \sqrt{\frac{1}{n}\sum_{i=1}^{n} XR_i^2}$$

$$R_y = \sqrt{\frac{1}{n}\sum_{i=1}^{n} YR_i^2}$$

$$T = \sqrt{R_x^2 + R_y^2} \quad or \quad \sqrt{\frac{1}{n}\sum_{i=1}^{n} XR_i^2 + YR_i^2}$$

Equation (3.26)

Where:

R_x = X RMS error

R_y = Y RMS error

T = total RMS error

n = the number of GCPs

i = GCP number

XR_i = X residual for GCP_i

YR_i = Y residual for GCP_i

3.6 Minimum Number of GCPs

Higher orders of transformation can be used to correct more complicated types of distortion. However, to use a higher order of transformation, more GCPs are needed. For instance, three points define a plane. Therefore, to perform a 1st order transformation, which is expressed by the equation of a plane, at least three GCPs are needed. Similarly, the equation used in a 2nd order transformation is the equation of a paraboloid, Six points are required to define a paraboloid. Therefore, at least six GCPs are required to perform a 2nd order transformation. The minimum number of points required to perform a transformation of order t equals (Intergraph Corporation, 2013):

$$= \frac{((t+1)(t+2))}{2}$$

Equation (3.27)

Use more than the minimum number of GCPs whenever possible. Although it is possible to get a perfect fit, it is rare, no matter how many GCPs are used.

For 1st- through 10th-order transformations, the minimum number of GCPs required to perform a transformation is listed in the following table (Intergraph Corporation, 2013):

Table 3.1: Minimum number of GCPs required to perform a transformation

Order of Transformation	Minimum GCPs Required
1	3
2	6
3	10
4	15
5	21
6	28
7	36
8	45
9	55
10	66

38

3.7 Resampling Methods

The next step in the rectification and registration process is to create the output file. Since the grid of pixels in the source image rarely matches the grid for the reference image, the pixels are resampled so that new data file values for the output file can be calculated (Intergraph Corporation, 2013).
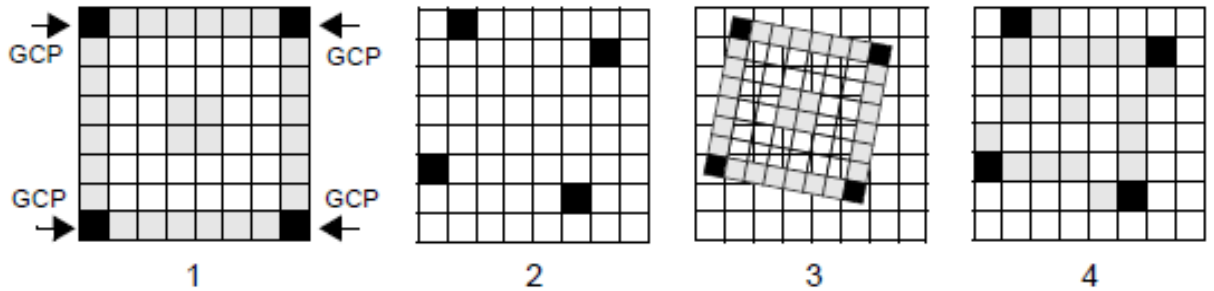
Figure 3.6 Resampling process

At Figure 3.6, the resampling process steps are as follows:

1. Grid 1 shows the input image containing source GCPs.

2. Grid 2 shows the output grid containing reference GCPs.

3. To compare the two grids, the input image is laid over the output grid so that the GCPs of the two grids fit together.

4. Using a resampling method, the input image pixel values are assigned to pixels in the output grid.

The following resampling methods are used at rectification process (Baboo and Devi, 2011):

- Nearest Neighbor: uses the value of the closest pixel to assign to the output pixel value as followed at Figure 3.7.

39
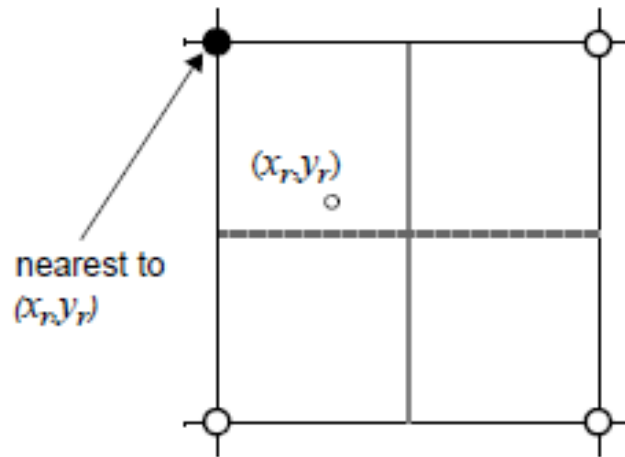
Figure 3.7 Nearest Neighbor Resampling Process

- <u>Bilinear Interpolation</u>: uses the data file values of four pixels in a 2×2 window to calculate an output value with a bilinear function as followed at Figure 3.8.
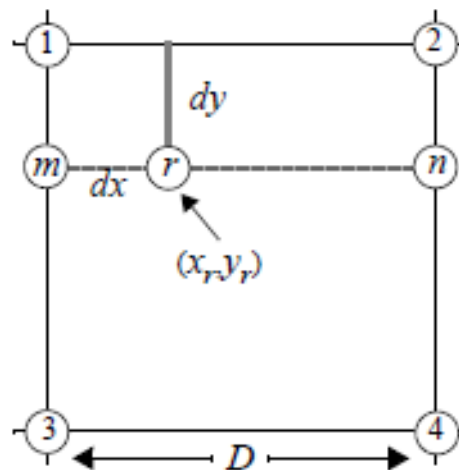
Figure 3.8 Bilinear Interpolation Resampling Process

- <u>Cubic Convolution</u>: uses the data file values of sixteen pixels in a 4×4 window to calculate an output value with a cubic function as followed at Figure 3.9.

40
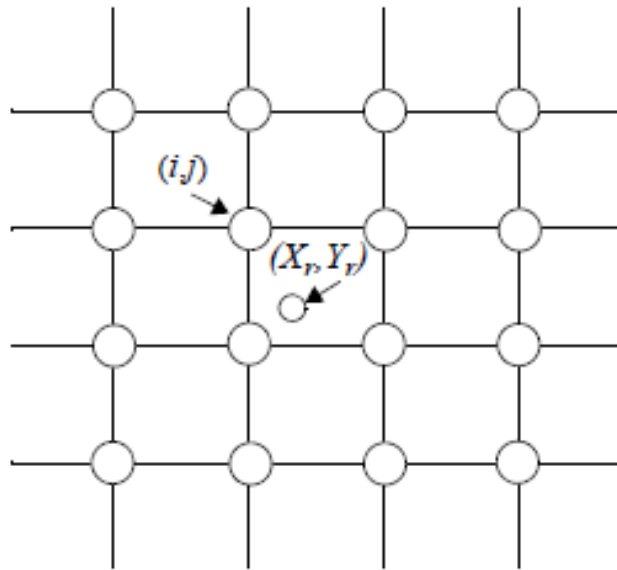
Figure 3.9 Cubic Convolution Resampling Process

- Bicubic Spline Interpolation: fits a cubic spline surface through the current block of points as followed at Figure 3.10.
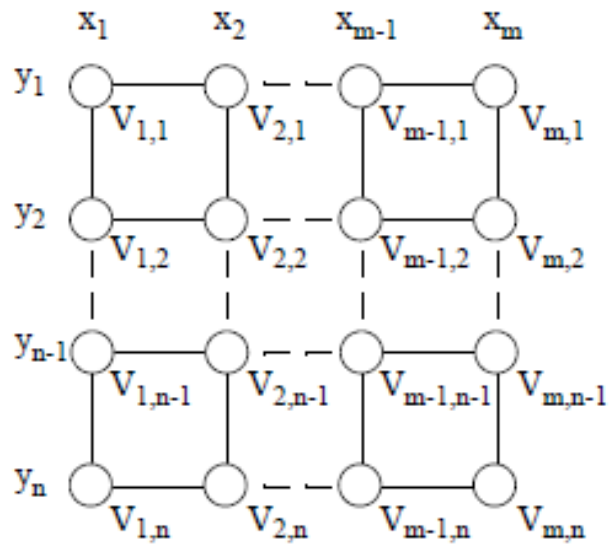
Figure 3.10 Bicubic Spline Interpolation Resampling Process

41

3.8   The Rectification Process

Remote sensing imagery requires spatial distortion corrections to maximize its usefulness for information extraction. The distortion arises from scanner characteristics and their interaction with the airborne platform or satellite orbital geometry and figure of the earth.

In correcting for distortion, we must essentially reposition pixels from their original locations in the data array into a specified reference grid. There are three components to the process:

- Selection of suitable mathematical distortion model.

- Coordinate transformation.

- Resampling (interpolation).

These three components are collectively known as warping (Wolberg, 1990).

With the increasing complexity of remote sensing systems, some having significant off nadir viewing capability, the interest in multisensor image registration, and the increasing demands of earth scientists for precision, temporal resolution, and repeatability in remote sensing measurements, there is a continuing need for geometric processing algorithms that are more accurate, autonomous, and efficient. Various terms are used to describe geometric correction of imagery, and it is worthwhile defining them before proceeding (Schowengerdt, 2007):

- Registration: The alignment of one image to another image of the same area. Any two pixels at the same location in both images are then "in register" and represent two samples at the same point on the earth .

- Rectification: The alignment of an image to a map so that the image is planimetric, just like the map . Also known as georeferencing .

- Resampling: Is the process of extrapolating data values for the pixels on the new grid from the values of the source pixels.

- Geocoding : A special case of rectification that includes scaling to a uniform, standard pixel. The use of standard pixel sizes and coordinates permits convenient "layering" of images from different sensors and maps in a GIS .

43

4 CHAPTER 4: MEHODOLOGY AND EXPERIMENTAL WORK

4.1 Scope

This chapter consists of three sections. It involves description of the study area which discusses the position of the study area which is Gaza City. Also, this chapter will involve the data available such as the image of Gaza City and the Ground Control Points. After that, The process of the rectification will start using the mathematical models with the software of ERDAS IMAGINE 2014.

4.2 Study Area

Gaza City is a coastal city located at latitude (31.3 degree) north, and longitude (34.18 degree) east, with an area of 56 km^2 approximately, and population of 600,000 inhabitants until 2015 (Figure 4.1) and (Figure 4.2). The primary economic activities of Gaza are small scale industries, agriculture and labor. However, the economy has been devastated by the blockade and recurring conflicts. Gaza has a very young population with roughly 75% being under the age of 25, and today the city has one of the highest population densities in the world. In a recent division of Gaza Municipality, Gaza City consists of Seventeen residential districts (Gaza Municipality website, 2015).

Gaza City is a sample that can be applied in all Gaza Strip of the rectification process, and the rectification which we do to Gaza City can be done for other governorates to get a corrected coordinate image of Gaza Strip.
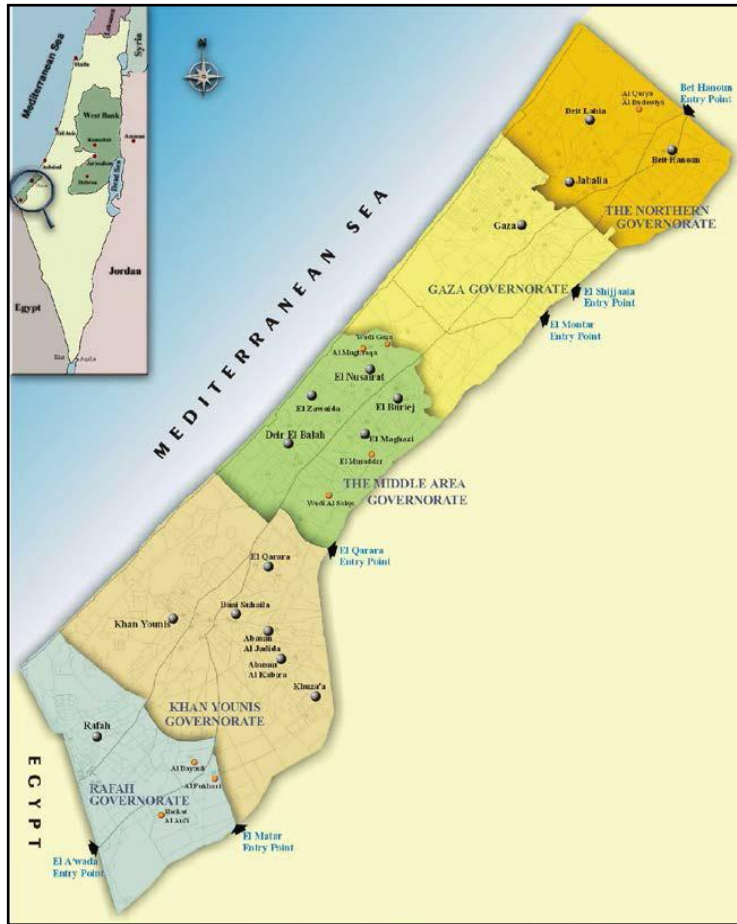
Figure 4.1: Gaza Strip Governorates
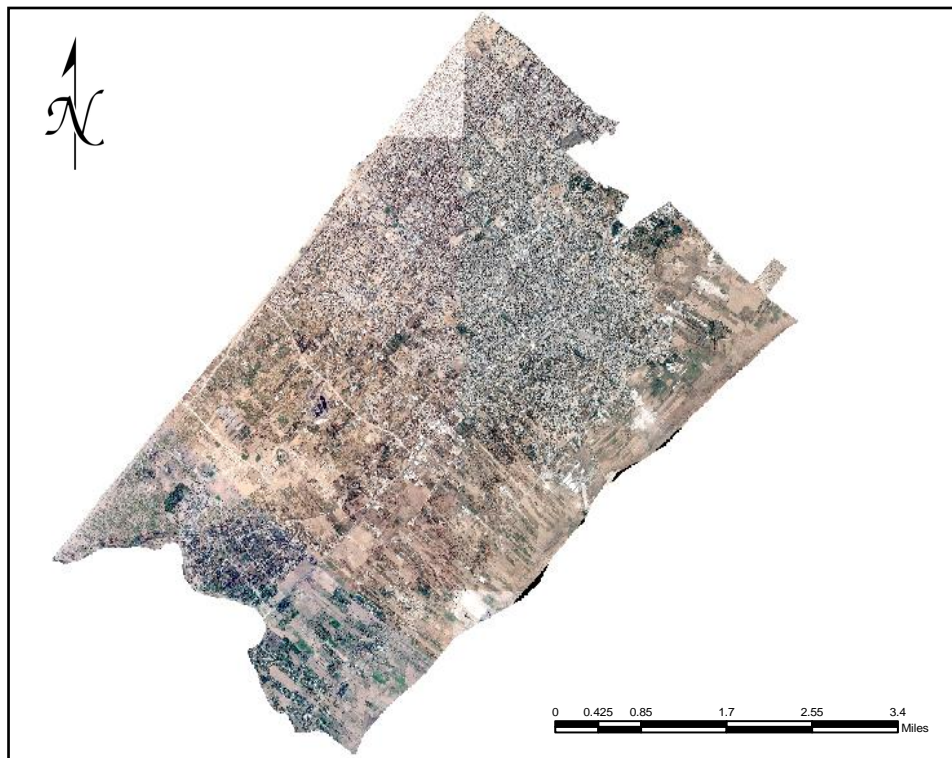
Figure 4.2: Gaza City Satellite Image

45

4.3 Ground Control Points

Ground Control Points are features of known ground locations that can be accurately located on the digital imagery. The GCPs must be well distributed and their locations must be easily identified. So, each GCP must be chosen in recognized locations.

Also its important to select number of points through the boarders of the image to ensure optimum horizontal rectification .

The GCPs consist of two X,Y pairs of coordinates and during the rectification process, the following terms will be identified:

- Source coordinates: usually data file coordinates in the image being rectified.

- Reference coordinates: the coordinates of the reference image or shape file to correct the image.

Collecting of GCPs was the second step after obtaining the image. So, the locations of these points were selected to be well known and easy to recognized. These locations generally include building corners and corners of walls that easily and accurate to locate it and not affected of other parameters at the image which may reduce the probability of locating it such as the shadow of the tall buildings.

For Gaza City, 38 ground control points are collected. These points are well distributed around the Gaza City; 26 of these points are control points to use for rectification process and the other 12 points are check points to use for evaluating the rectification accuracy process.

(Table 4.1) shows the GCPs with their locations (X,Y) at the actual earth surface with Palestine 1923 Grid coordinate system, and their points collected depending on Municipality of Gaza GCPs which are fixed at accurate locations with known coordinates.

46

Tabel 4.1 : The GCPs of Gaza City

Point ID	X(m)	Y(M)	Type
P1	98334.652	106047.026	Control
P2	98221.713	106128.814	Check
P3	97793.21	98429.783	Control
P4	97681.639	98470.407	Control
P5	97755.768	98534.093	Check
P6	93282.877	99959.753	Control
P7	93265.304	99941.083	Control
P8	93198.351	99875.563	Control
P9	93226.088	99903.944	Check
P10	95197.283	97753.191	Control
P11	95155.517	97715.145	Control
P12	95173.041	97695.914	Check
P13	96578.564	104078.998	Control
P14	96571.216	104017.384	Control
P15	96535.897	103977.375	Check
P16	97342.567	103579.592	Control
P17	101656.557	101396.79	Check
P18	101680.322	101435.054	Control
P19	99776.668	104889.114	Control
P20	98629.689	103923.046	Control
P21	101543.833	100504.043	Check
P22	101131.245	100758.096	Control
P23	95773.494	102879.45	Control
P24	96402.374	102379.262	Control
P25	96372.472	102402.706	Check
P26	96291.533	102408.534	Control
P27	97107.81	101570.286	Control
P28	98454.66	101016.762	Control
P29	99166.076	100001.733	Control
P30	99267.575	99994.906	Check
P31	99875.323	99295.038	Control
P32	99895.133	99141.518	Check
P33	94166.541	101029.064	Control
P34	94103.518	101009.03	Check
P35	95702.629	99892.546	Control
P36	96596.915	101125.68	Check
P37	97481.343	100364.498	Control
P38	101109.52	102650.995	Control

47

After collecting the well distributed control points, they are located on the image of Gaza City as mentioned (Figure 4.3); where the control points used at the rectification process with red color and the check point with blue color.
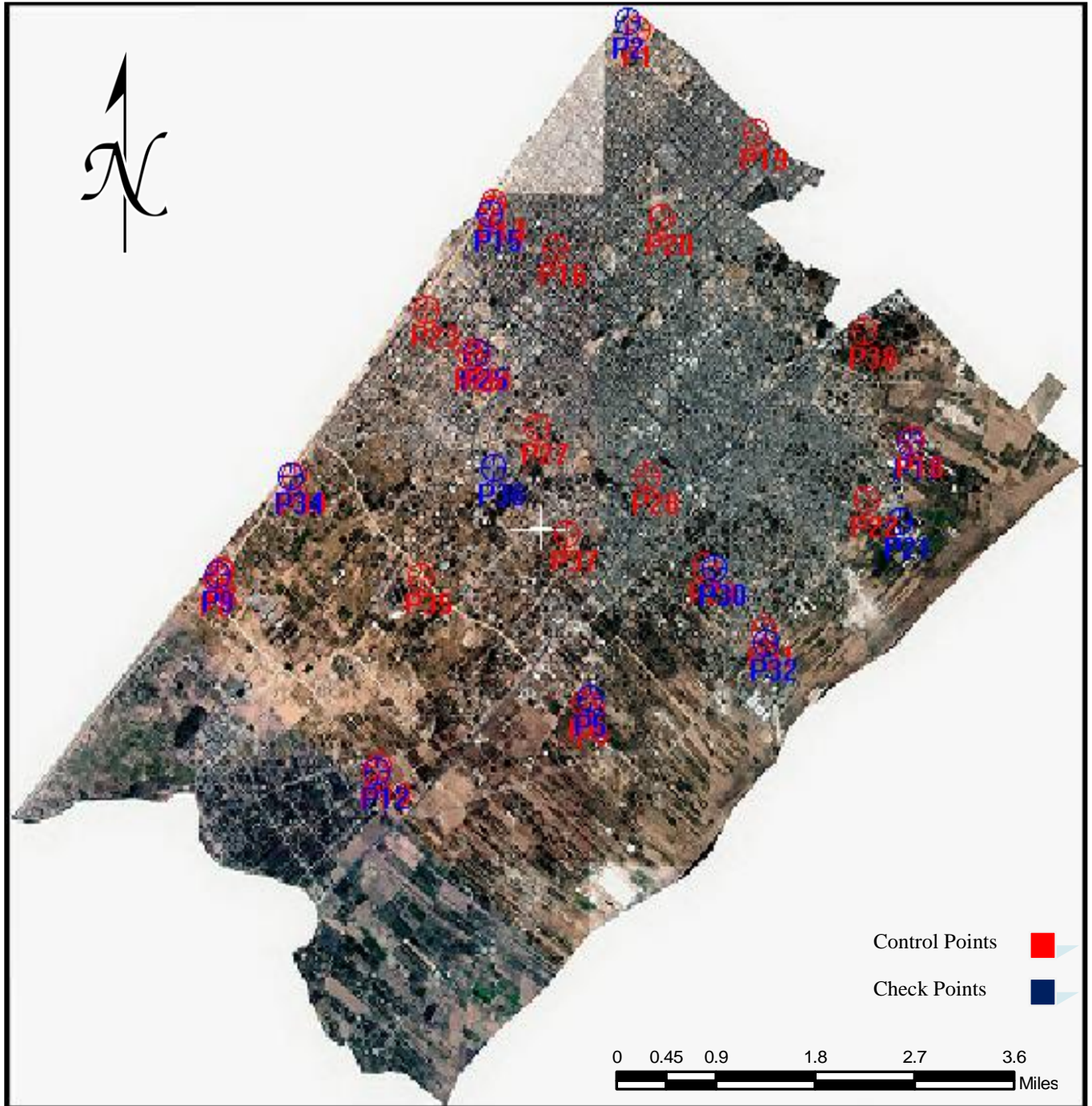
Figure 4.3: Gaza City satellite image with GCPs

4.4   The Rectification Process

To apply the rectification process on the satellite image , the related GCPs must be divided to two groups; the first group includes the GCPs that are used in the rectification process, and the other will used as check points to evaluate the accuracy resulted from rectification process.

With Gaza City image, use 38 GCPs are used divided to 26 control points and 12 check points as mentioned for rectification process using the two dimensional mathematical models.

At rectifying the Gaza City image, the basic steps used are:

- Display files which contain the uncorrected image at Erdas Imagine Program.

- Starting Geometric Correction Tool.

- Record and register GCPs.

- Compute a transformation models matrix.

- Resample the image.

- Verify the rectification process.

By using ERDAS IMAGINE program , the models of the software are; first order Polynomial , Second order Polynomial, Third order Polynomial, Fourth order Polynomial, First order Projective Transformation, second order Projective Transformation and third order Projective Transformation.

(Figure 4.4) shows the rectification process framework.

49
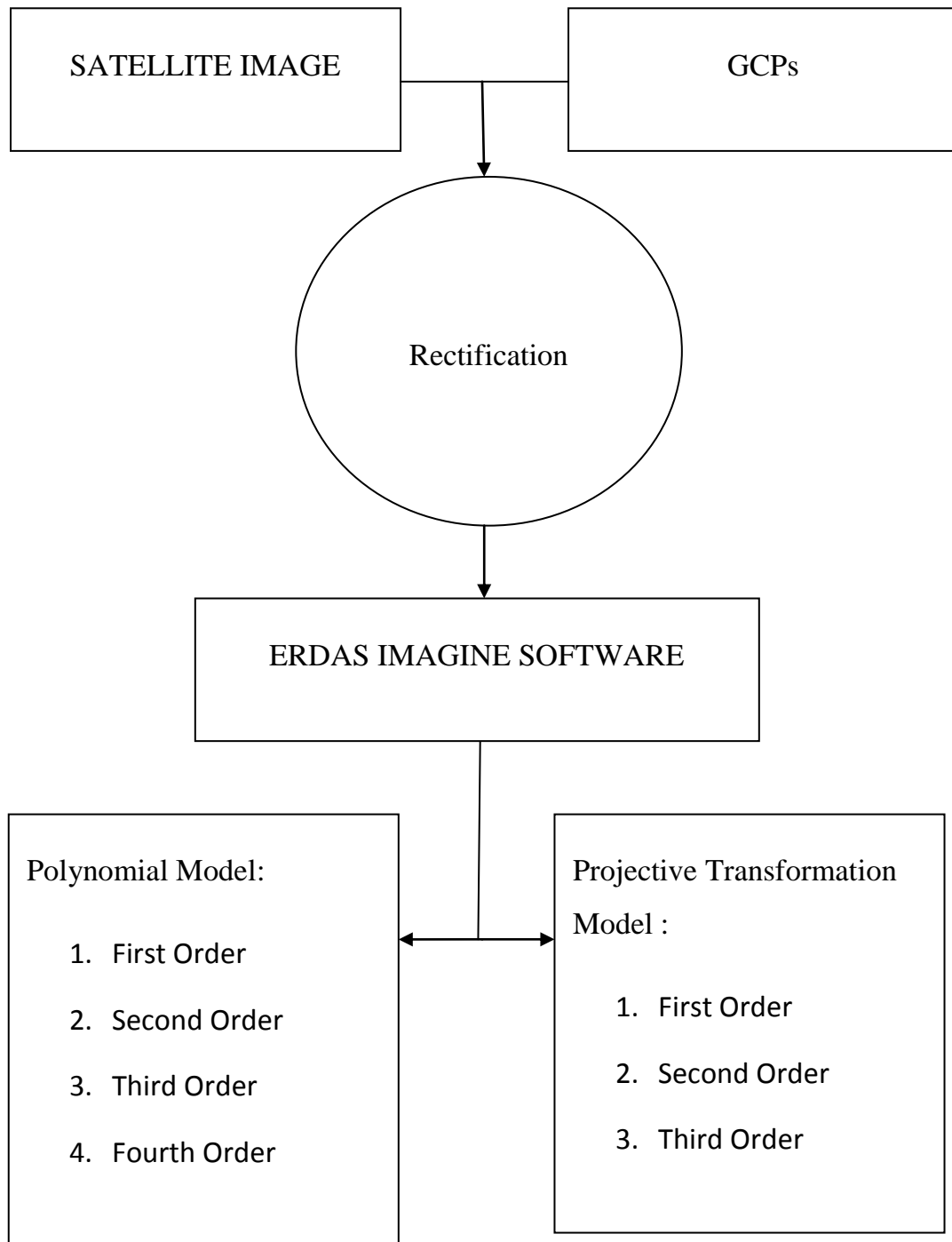
Figure 4.4: Rectification Process Diagram

50

4.4.1 Experimental Work

The following tables include the results of rectification process on the image in the case of using 26 GCPs for rectification and 12 GCPs for check.

Firstly, the process done for different orders of polynomial mathematical models.

Table 4.2 : First order polynomial rectification

Point ID	ΔX (m)	ΔY (m)	RMSE(m)
P2	-1.06	-0.536	1.187
P5	1.017	0.238	1.045
P9	-1.03	1.48	1.804
P12	0.273	-0.645	0.7
P15	-0.124	-0.624	0.636
P17	1.248	-0.399	1.31
P21	0.2	-0.309	0.368
P25	0.821	0.177	0.84
P30	0.62	0.684	0.923
P32	0.105	-0.639	0.648
P34	-0.257	-0.919	0.954
P36	-0.095	-0.424	0.435
Total RMSE	0.7102	0.6787	0.9823

Table 4.2 shows that the first order polynomial rectification resulted the accuracy of 0.7102 m in the X direction , 0.6787 m in the Y direction and total root mean square error (RMSE) is 0.9823 m.

Table 4.3 : Second order polynomial rectification

Point ID	ΔX (m)	ΔY (m)	RMSE(m)
P2	-0.451	-0.469	0.651
P5	0.9	0.247	0.933
P9	-0.683	1.609	1.748

51

Point ID	ΔX (m)	ΔY (m)	RMSE(m)
P12	0.626	-0.932	1.123
P15	-0.263	-0.425	0.5
P17	1.588	-0.145	1.595
P21	0.493	0.19	0.528
P25	0.455	0.161	0.483
P30	0.393	0.746	0.843
P32	0.09	-0.233	0.25
P34	-0.285	-0.72	0.774
P36	-0.512	-0.59	0.782
Total RMSE	0.672	0.6758	0.9531

Table 4.3 shows that the second order polynomial rectification resulted accuracy 0.6720 m in the X direction and 0.6758 m in the Y direction and the total RMSE is 0.9531 m which these results have been improved due to the previous first order polynomial .

Table 4.4 : Third order polynomial rectification

Point ID	ΔX (m)	ΔY (m)	RMSE(m)
P2	-0.172	-0.632	0.655
P5	1.31	0.017	1.31
P9	-0.514	1.297	1.395
P12	0.087	-0.38	M 0.39
P15	-0.487	-0.054	0.49
P17	1.165	0.394	1.23
P21	-0.206	0.424	0.472
P25	0.266	0.279	0.385
P30	0.68	0.431	0.805
P32	0.146	-0.799	0.812
P34	0.029	-0.731	0.732
P36	-0.544	-0.596	0.807
Total RMSE	0.6128	0.6025	0.8594

52

Table 4.4 shows that the third order polynomial rectification resulted accuracy 0.6128 m in the X direction and 0.6025 m in the Y direction and the total RMSE is 0.8594 m, the results at this order is more accurate than first and second order polynomial.

Table 4.5 : Fourth order polynomial rectification

Point ID	ΔX (m)	ΔY (m)	RMSE(m)
P2	0.111	-0.042	0.119
P5	0.831	-0.427	0.934
P9	-0.61	1.161	1.311
P12	0.245	-0.189	0.31
P15	-0.2	0.029	0.202
P17	0.794	-0.001	0.794
P21	1.218	1.724	2.111
P25	-0.086	0.023	0.089
P30	0.21	-0.201	0.291
P32	1.522	0.58	1.629
P34	0.277	-0.227	0.358
P36	-0.332	-0.36	0.489
Total RMSE	0.6979	0.6519	0.955

Table 4.5 shows that the fourth order polynomial rectification resulted accuracy 0.6979 m in the X direction, 0.6519 m in the Y direction and the total RMSE is 0.955 m.

It is clear that by using Erdas Imagine Program with the Gaza City image and the same GCPs, the third order polynomial rectification get the best spatial accuracy.

Secondly, the process done for different orders of projective transform mathematical models with the same image and GCPs.

Table 4.6 : First order projective transform rectification

Point ID	ΔX (m)	ΔY (m)	RMSE(m)
P2	-1.067	-0.416	1.145
P5	0.917	0.236	0.947

53

Point ID	ΔX (m)	ΔY (m)	RMSE(m)
P9	-0.886	1.498	1.741
P12	0.265	-0.522	0.586
P15	-0.185	-0.671	0.696
P17	1.621	-0.732	1.779
P21	0.327	-0.358	0.485
P25	0.757	0.117	0.766
P30	0.571	0.638	0.856
P32	0.069	-0.7	0.703
P34	-0.208	-0.969	0.991
P36	-0.166	-0.469	0.497
Total RMSE	0.7405	0.7029	1.021

Table 4.6 shows that the first order projective transform model resulted accuracy 0.7405 m in the X direction, 0.7029 m in the Y direction and the total RMSE is 1.021 m.

Table 4.7 : Second order projective transform rectification

Point ID	ΔX (m)	ΔY (m)	RMSE(m)
P2	-0.593	-0.296	0.662
P5	0.914	0.085	0.918
P9	-0.606	1.765	1.866
P12	0.622	-0.498	0.797
P15	-0.405	-0.367	0.547
P17	1.612	-0.576	1.712
P21	0.498	-0.061	0.502
P25	0.618	0.172	0.642
P30	0.628	0.704	0.944
P32	0.253	-0.692	0.737
P34	-0.424	-0.774	0.882
P36	-0.199	-0.471	0.512
Total RMSE	0.7078	0.6925	0.9902

54

Table 4.7 shows that the second order projective transform rectification resulted accuracy 0.7078 m in the X direction, 0.6925 m in the Y direction and the total RMSE is 0.9902 m.

Table 4.8 : Third order projective transform rectification

Point ID	ΔX (m)	ΔY (m)	RMSE(m)
P2	-0.726	-0.686	0.999
P5	0.934	-0.021	0.935
P9	-0.554	1.345	1.455
P12	0.469	-0.456	0.654
P15	-0.467	-0.081	0.474
P17	1.264	0.074	1.266
P21	-0.02	0.469	0.469
P25	0.617	0.341	0.705
P30	0.577	0.738	0.937
P32	0.157	-0.833	0.847
P34	-0.189	-0.703	0.728
P36	-0.198	-0.443	0.485
Total RMSE	0.6162	0.6303	0.8814

Table 4.8 shows that the third order projective transform rectification resulted accuracy 0.6162 m in the X direction, 0.6303 m in the Y direction and the total RMSE is 0.8814 m .

It's clear that the third order projective transform model rectification get the best spatial accuracy at the model but the best accuracy at all the orders and models is the third order polynomial.

55

Table 4.9 summarizes the final results using different orders of polynomial model with the RMSE for every order and expressed at the Figure 4.5.

Table 4.9 : The final results of rectification using polynomial models

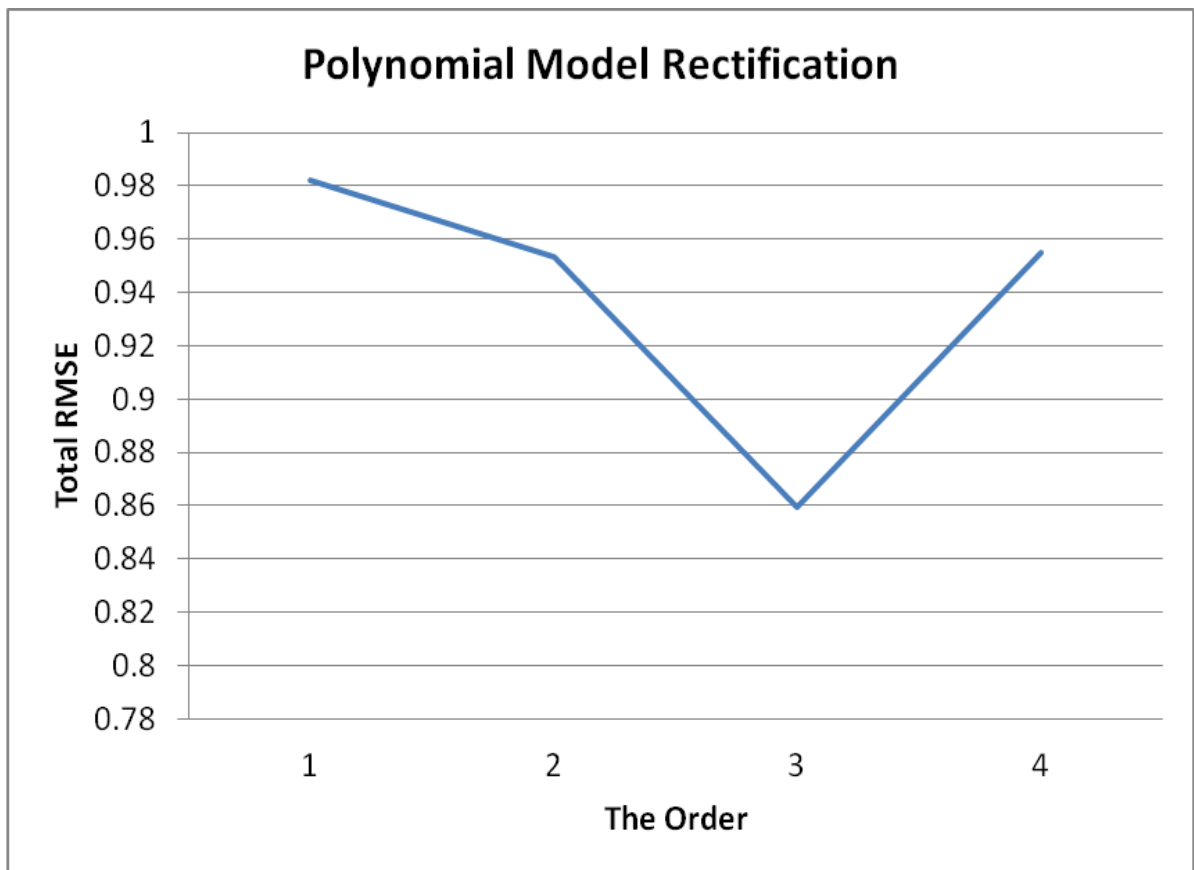| Model	Polynomial							
	1'st		2'nd		3'rd		4'th	
RMSE	rmsx	rmsy	rmsx	rmsy	rmsx	rmsy	rmsx	rmsy
Values	0.7102	0.6787	0.672	0.6758	0.6128	0.6025	0.6979	0.6519
Total RMSE	0.9823		0.9531		0.8594		0.955	

Figure 4.5: Rectification process (polynomial models)

56

Table 4.10 summarizes the final results using different orders of project transform model with the RMSE for every order and expressed at the Figure 4.6.

Table 4.10 : The final results of rectification using projective transform models

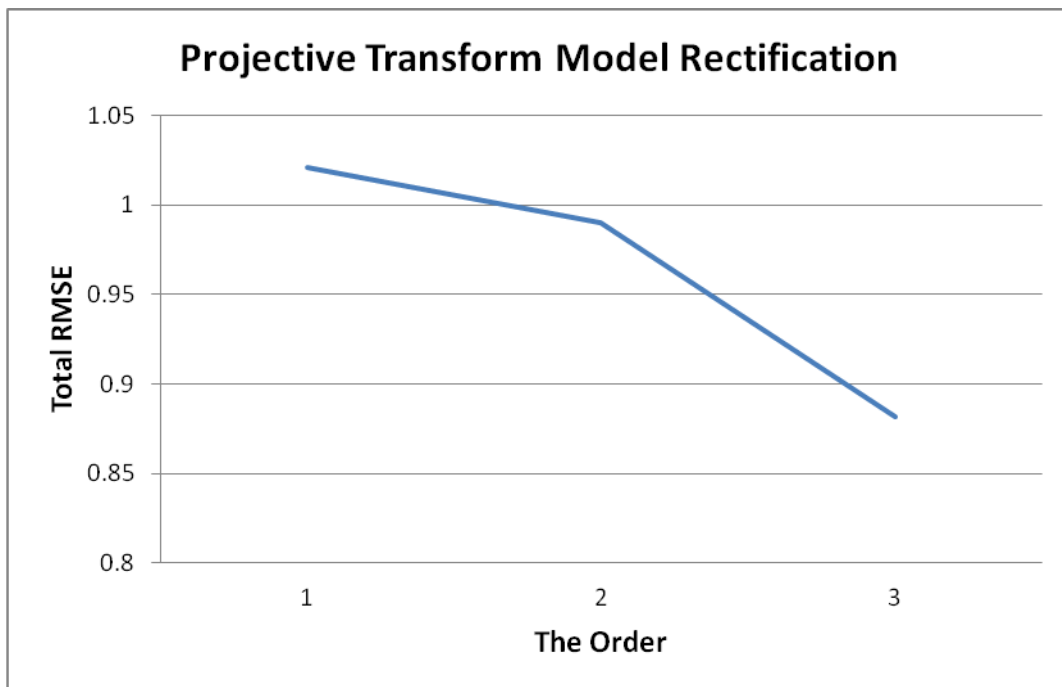| Model	Projective Transformation					
	1'st		2'nd		3'rd	
RMSE	rmsx	rmsy	rmsx	rmsy	rmsx	rmsy
Values	0.7405	0.7029	0.7078	0.6925	0.6162	0.6303
Total RMSE	1.021		0.9902		0.8814	

Figure 4.6: Rectification process results (projective models)

From previous experiments and as showing at table (4.10) and table (4.11), also by comparing the models used at the rectification process, and by using the polynomial and projective transform models, it's clear that the third order in each model has the best accuracy in addition to the preference of the third order polynomial model which have the best accuracy of RMSE 0.8594 m.

57

The computation and output of a higher order polynomial equation are more complex than that of a lower order polynomial equation. Therefore, higher order polynomials are used to perform more complicated image rectifications.

The following example uses only one coordinate (X), instead of two (X,Y), which are used in the polynomials for rectification. This enables you to draw two-dimensional graphs that illustrate the way that higher orders of transformation affect the output image.
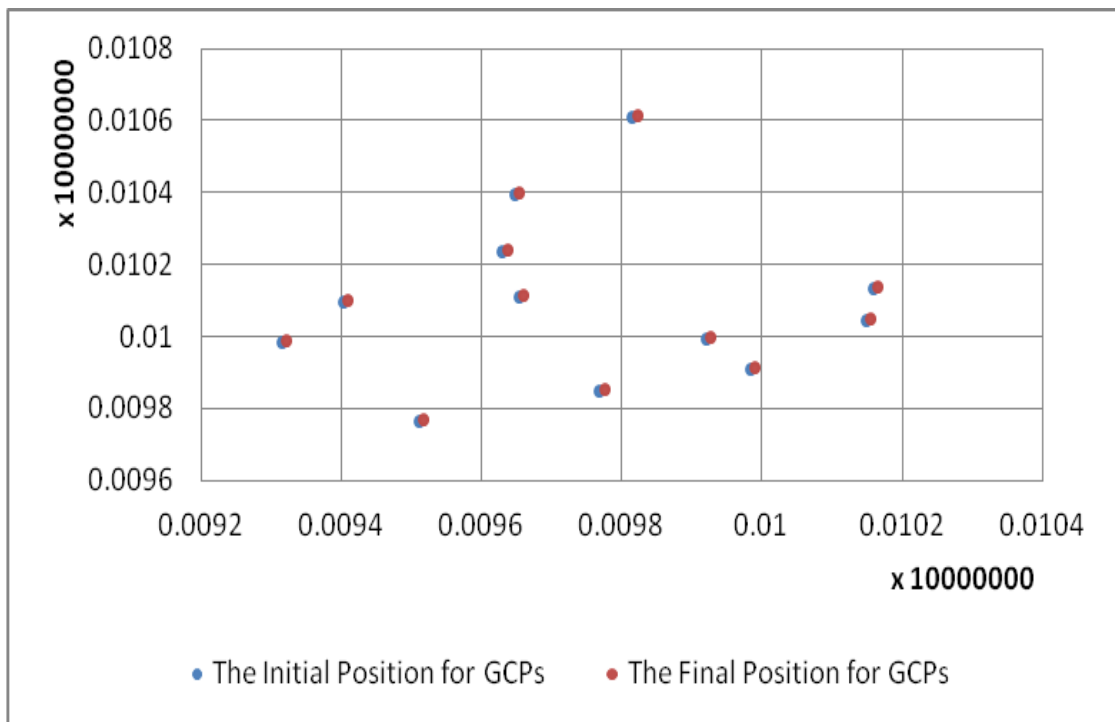

Figure 4.7: The final rectification process results

4.4.2 The Effect of GCPs Number on the Rectification Process

To define the effect of the GCPs number on the attainable accuracy of rectification process, this operation is performed by different number of GCPs with the best mathematical model resulted - third order polynomial- and by reducing the number of the GCPs each step,and all that by using Erdas Imagine program.

The results are as the following tables for the image.

58

Table 4.11 : The Effect of GCPs number on the rectification process

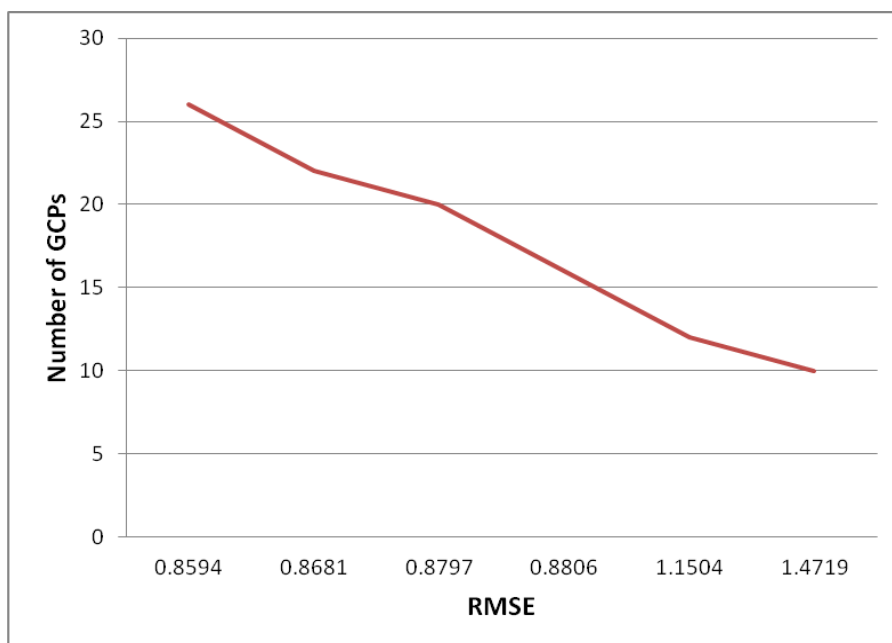| GCPs Number	RMSx	RMSy	RMSE
26	0.6128	0.6025	0.8594
22	0.6338	0.5932	0.8681
20	0.6247	0.6193	0.8797
16	0.6374	0.6076	0.8806
12	0.5538	1.0084	1.1504
10	0.8925	1.1705	1.4719

Figure 4.8: The Effect of GCPs number on the rectification process

59

5 CHAPTER 5: CONCLUSION AND RECOMMENDATIONS

5.1 Conclusion

For the Rectification Process :

The results can be concluded from the research at the following points :

- The Third order polynomial model using Erdas Imagine Programe gives the best spatial accuracy in the rectification process but for a last study of A.Al Yossof, he found that second order polynomial model gives the highest spatial accuracy, and the difference between these studies depending on the area covered , the number of GCPs, the resolution of the image and the model which the research of the study used the second order polynomial for the Quickbird model, these factors have an effective effect on the results.

- According to the order of the polynomial model we used , the minimum number of GCPs was 12 point to do the process, but by applying the rectification process with well distributed different number of the GCPs. It's found that the number of the GCPs is related with the accuracy of the process, so when the number of GCPs increases, the total RMSE will decrease and the same result were at the study of F. Eltohamy and E. H. Hamza.

- The resolution of the image effect on the rectification process, so using an image of higher resolution will give better results.

- The location of the GCPs must be well knows points, so by locating these points at the corners of the walls and at the intersection will give us best accuracy than using points at several buildings which may the effect of the sun shadow and have a negative effect of locating the GCPs and the same result were at the study of F. Eltohamy and E. H. Hamza but they also studied the effect of locating bad point at the image.

5.2 Recommendations

- For Gaza City and Gaza Strip, Its recommended to use the third order polynomial in the rectification process because it gives the highest accuracy results.

- Its recommended also not to satisfy with using the minimum number of GCPs , but using well distributed GCPs with a number which give me the best accuracy.

- As an extension of this research I recommend :

1. Apply the rectification process for Gaza Strip by using satellite image and GCPs along the Strip.

2. Apply an orthorectification process on the Gaza City .

3. Modify models that to have better accuracy.

4. Depending on the rectification process, I recommend to apply the feature extractions from the rectified image .

61

REFERENCES

A Canada Centre for Remote Sensing., 2007 . Fundamentals of Remote Sensing . Canada Centre for Remote Sensing , Natural Resources, Canada.

Aggarwal, S., 2003. Principles of remote sensing. Photogrammetry and Remote Sensing Division, Indian Institute of Remote Sensing, Dehra Dun.

Amin, H., 2004. Potential Accuracy of Point Positioning Using High Resolution Satellite Imagery, Zagazig University, Banha branch.

Amini, J. and Hashemi, A.,2005. Geometric Correction in Ikonos Images – Case Study: Tehran, Iran, FIG Working Week 2005 and GSDI-8 Cairo, Egypt April 16-21.

Al Yousef, A.,2004. Two Dimentional Rectification for QuickBird Satellite Image, Cairo University.

Baboo, S. and Devi, M., 2011. Geometric Correction in Recent High Resolution Satellite Imagery: A Case Study in Coimbatore, Tamil Nadu, International Journal of Computer Applications (0975 – 8887) Volume 14– No.1.

Baboo, S. and Thirunavukkarasu, S., 2014. Geometric Correction in High Resolution Satellite Imagery using Mathematical Methods: A Case Study in Kiliyar Sub Basin., Global Journals Inc, Volume 14 Issue 1 Version 1.0 ,USA.

Barker, R. Kirk, J. and Munday, R.J., 1988. Narrative analysis 3rd ed. Bloomington, Indiana University Press.

Boughton, J.M., 2002. The Bretton Woods proposal: an indepth look. Political Science Quarterly, 42(6), pp.564-78.

Choo, A. L. Chan, Y. K. and Koo, V. C., 2012. Geometric Correction on SAR Imagery, Progress In Electromagnetic Research Symposium Proceedings, KL, MALAYSIA, March 27-30.

Clarke, K. C., 2001. Getting Started With Geographic Information Systems, Third Edition. Prentice Hall, Upper Saddle River, NJ.

ELtohamy, F. and Hamza, E.h., 2009. Effect of Ground Control points Location and Distribution on Geometric Correction Accuracy of Remote Sensing Satellite Images. 13th International Conference on AEROSPACE SCIENCES & AVIATION TECHNOLOGY, Military Technical College, Kobry ElKobbah, Cairo, Egypt.

Fraser, S., 2000. High Resolution Satellite Imagery: A Review of Metric Aspects, , International Archives of Photogrammetry and Remote Sensing. Vol. XXXIII, Part B7. Amsterdam.

Gaza Municipality Site, 2015. [online] Available at: www.gaza-city.org [Accessed 25 October 2015].

Guang, Y. and Weili, J., 2011. Research on Impact of Ground Control Point Distribution on Image Geometric Rectification Based on Voronoi Diagram , Published by Elsevier Ltd. , Procedia Environmental Sciences 11 (2011) 365 – 371.

Intergraph Corporation, 2013. Erdas Imagine Field Guide, United States.

Japan Association of Remote Sensing, JARS,. 1999. Remot Sensing Notes , Asian Center for Research on Remote Sensing (ACRoRS) , Asian Institute of Technology (AIT).

Kumar, M., 2003. Digital Image Processing, Indian Institute of Remote Sensing, Satellite Remote Sensing and GIS Applications in Agricultural Meteorology p. 81-102, Dehra Dun.

Levin, N., 1999. Fundamentals of Remote Sensing. Tel Aviv University.

Ok, A. O. and Turker, M., 2005. Comparison of Different Mathematical Models on the Accuracy of the Orthorectification of Aster Imagery, Hacettepe University, Faculty of Engineering, Department of Geodesy and Photogrammetry, 06800, Beytepe, Ankara, Turkey.

Oslen, R.C., 2007. Remote Sensing from Air and Space, SPIE—The International Society for Optical Engineering, Bellingham, Washington.

Panigrahi, N. Mohan, B.K. and Athithan, G., 2011. Pre-processing Algorithm for Rectification of Geometric Distortions in Satellite Images. Defence Science Journal, Vol. 61, No. 2, March 2011, pp. 174-179

Poli, D. and Toutin, T., 2012. Review of Developments In Geometric Modeling for High Resolution Satellite Pushbroom Sensors. The Photogrammetric Record 27(137): 58–73.

Sanderson, R.S., 2001. Introduction to Remote Sensing. New Mexico State University.

Schowengerdt, R., 2007. Remote Sensing: Models and Methods for Image Processing, third edition, Library of Congress Cataloging-in-Publication Data, USA.

Spath, H.,2004. A numerical method for determining the spatial HELMERT transformation in the case of different scale factors, Zeitschrift fur Vermessungswesen 129, p 255-259.

Wang, F. and Shi, W., 2001 . Partial Distortion Correction of Remote Sensing Image Rectification Error. Hong Kong government , Development of infrastructure for Cyber Hong Kong.

Weng, Q., 2010. Remote Sensing and GIS Integration, McGraw-Hill Companies, Inc

Wikipedia Site (2014), "Erdas Imagine", Available at:
http://en.wikipedia.org/wiki/Erdaas_Imagine [accessed on November 16th, 2014].

Wikipedia Site (2015), "Remote Sensing", Available at:
http://en.wikipedia.org/wiki/Remote_Sensing [accessed on March 10th, 2015].

Zhang, J.Z., 2000. Strict Geometric Model Based on Affine Transformation for Remote Sensing Image with High Resolution. The International Society for Photogrammetry and Remote Sensing ISPRS, http://www.isprs.org/proceedings/xxxiv/part3/papers/paper168.pdf [Accessed 06 October 2015].

Zhou, G. and Li, R., 2000. Accuracy Evaluation of Ground Points from IKONOS High-Resolution Satellite Imagery, Photogrammetric Engineering end Remote Sensing, volume 66, number 9, September.

Zhu, C. JIN, J. and XU, Q ., 2002, Fast Rectification For Space-Born SAR Digital Image with No Ground Control Point, IAPRS, volume XXXEV, pan 2. commission H, Xian, August 20-23.

Zoej, M.J. Mansourian, A. Mojardi B and Sadighian, S.,2002. 2D Geometric Correction of IKONOS Imagery using Genetic Algorithms. Symposium of Geospatial Theory , Processing and Applications, Ottawa.